ABSTRACT

FREQUENCY-SELECTIVE DESIGN OF WIRELESS POWER TRANSFER SYSTEMS FOR CONTROLLED ACCESS APPLICATIONS

by Tyler Stephen Maschino

Wireless power transfer (WPT) has become a common way to charge or power many types of devices, ranging from cell phones to electric toothbrushes. WPT became popular through the introduction of a transmission mode known as strongly coupled magnetic resonance (SCMR). This means of transmission is non-radiative and enables mid-range WPT. Shortly after the development of WPT via SCMR, a group of researchers introduced the concept of resonant repeaters, which allows power to hop from the source to the device. These repeaters are in resonance with the WPT system, which enables them to propagate the power wirelessly with minimal losses to the environment. Resonant repeaters have rekindled the dream of ubiquitous wireless power. Inherent risks come with the realization of such a dream. One of the most prominent risks, which we set out in this thesis to address, is that of accessibility to the WPT system. We propose the incorporation of a controlled access schema within a WPT system to prevent unwarranted use of wireless power. Our thesis discusses the history of electromagnetism, examines the inception of WPT via SCMR, evaluates recent developments in WPT, and further elaborates on the controlled access schema we wish to contribute to the field.

FREQUENCY-SELECTIVE DESIGN OF WIRELESS POWER TRANSFER SYSTEMS FOR CONTROLLED ACCESS APPLICATIONS

A Thesis

Submitted to the

Faculty of Miami University

in partial fulfillment of

the requirements for the degree of

Master of Science in Computational Science and Engineering

Department of Electrical & Computer Engineering

by

Tyler Stephen Maschino

Miami University

Oxford, Ohio

2016

Advisor _____

Dr. Dmitriy Garmatyuk

Reader _____

Dr. Mark Scott

Reader _____

Dr. Herbert Jaeger

Contents

List of Tables

List of Figures

Chapter 1

Introduction and Motivation

Wireless power transfer (WPT) systems pervade the consumer electronics industry. However, WPT hasn't been around for all that long. Modern WPT came about largely as a result of the work of Nikola Tesla at the turn of the 19th century, but the journey to that point began with several fundamental discoveries in electricity and magnetism. In 1812, Karl Friedrich Gauss rediscovered Joseph-Louis Lagrange's 1764 gravitational divergence theorem. He labeled it Gauss's divergence theorem and used it to derive the famous Gauss's law. Gauss's law states that the electric charge inside of a body is proportional to the electric field that permeates the space around it. In 1820, André-Marie Ampère demonstrated that current-carrying wires create an attractive or repellant force, depending on the direction of the currents within the parallel wires. This relationship is known as Ampère's force law. Shortly thereafter, in 1821, Michael Faraday found that a current-carrying wire creates a magnetic field. This magnetic field is the cause of attraction or repulsion of two parallel, current-carrying wires. Ampère published the results of his experimentation with magnetism in 1825. In his work, he describes an expression that relates the electric current passing through a loop to the integrated magnetic field in space around the loop. This discovery has become known as Ampère's circuital law. In 1831, Faraday determined that by varying the current along a wire, nearby circuits could experience induced currents. He explained this phenomenon, electromagnetic induction, using the concept of magnetic flux; a changing magnetic field, created by a changing current, can produce an induced current on a neighboring circuit. Interestingly, although Faraday is largely credited for developing his law of induction, Joseph Henry also discovered electromagnetic induction in 1831, but failed to publish his results [1].

In the autumn of 1855, a young Scottish mathematician, by the name of James Clerk

Maxwell, published his first paper, which included a section entitled "On Faraday's Lines of Force". In the publication, Maxwell outlines Faraday's findings in an explicit mathematical form using the vectorial analysis of the day. He derives these equations by assuming the lines of force to be a similar to the lines of flow of an incompressible fluid [1]. This analogy is used by Maxwell because of the fact "that partial similarity between the laws of one science and those of another [...] makes each of them illustrate the other" [2]. In 1861, Maxwell published Parts I and II of his newest paper, "On Physical Lines of Force"; Parts III and IV followed in 1862. It is in this publication that the tetrad of equations, which will ultimately be known as Maxwell's equations, can be found. Armed with these equations, Maxwell was better equipped to derive the electromagnetic (EM) wave equation. Maxwell published his research again in 1865 with a work entitled "A Dynamical Theory of the Electromagnetic Field". This paper was the first to utilize Faraday's field concept in mathematical form. Maxwell's research included in this paper was pivotal for the study of electromagnetism due to its derivation of the EM wave equation, deduction of the properties of EM waves from the field equations, and determination that light is actually comprised of EM waves. In this paper, he posits twenty equations in scalar form that contain twenty variables. In 1873, Maxwell published "A Treatise on Electricity and Magnetism" which served to synthesize his work in electricity and magnetism [1].

In the period before Heinrich Rudolf Hertz's death in 1894, Hertz and "The Maxwellians" (George Francis FitzGerald, Oliver Lodge, and Oliver W. Heaviside), as referred to by Heaviside, helped to bring about the scientific community's acceptance of Maxwell's theory. In 1883, FitzGerald proposed that testing Maxwell's theory could be accomplished by running an alternating current (AC) through a loop of wire. FitzGerald discovered that high frequency oscillating currents are required to test Maxwell's theory. He later suggested that such frequencies could be achieved by discharging a capacitor into the circuit. In 1884, Hertz found that the electric field created by charges is identical to the electric field created by a changing magnetic field. Building upon this discovery, Hertz further distilled Maxwell's original twenty equations in scalar form to twelve equations in scalar form by removing the concept of aether and rewriting the equations in terms of sources, instead of potentials. Heaviside, shortly thereafter in 1886, converted Maxwell's equations to vector form by utilizing the vector-based concepts of gradient, curl, and divergence. This simplification resulted in four equations in vector form, which can be seen in 1.1 [1]. These four equations are colloquially known today as "Maxwell's Equations".

Name	Differential Equation
Gauss's law	$\nabla \cdot \mathbf{D} = \rho$
Gauss's law for magnetism	$\nabla \cdot \mathbf{B} = 0$
Faraday's law of induction	$\nabla \times \mathbf{E} = -\frac{\delta \mathbf{B}}{\delta t}$
Ampere's law with Maxwell's correction	$\nabla \times \mathbf{H} = -\frac{\delta \mathbf{B}}{\delta t}$

Table 1.1: Maxwell's equations in vector form

It is also important to note that, during this time, the term impedance was introduced by Heaviside to refer to the quotient of voltage over current. In 1887, Hertz experimentally proved that radio waves exist. He found that ultraviolet light directed toward a spark gap's negative electrode enabled greater conduction by the gas in the gap between the electrodes. Then, in 1888, Hertz made another discover that was crucial to the acceptance of Maxwell's electromagnetic theory; he found that a secondary circuit can spark if the frequencies of the primary and secondary circuits are in resonance. This experiment showed that signals moving through the air and through wire propagate at approximately the same speed: the speed of light. Hertz also found that electric radiation diffracted when passing through a slit in a screen. This led to Hertz generating, transmitting, and identifying EM waves ranging in wavelength from 5 meters to 50 centimeters. These experiments confirmed Maxwell's theory of electromagnetism. Interestingly, Hertz and the Maxwellians were unaware of one another's work until Hertz published his paper in 1888. A year later, in 1889, Hertz presented his findings from his experimentation with his oscillating spark gap. In the same year, Heaviside and FitzGerald independently suggested that the speed of EM propagation will always be constrained by an upper bound: the speed of light. After publishing the findings from his experiments, Hertz continued to experiment with electromagnetism until passing away in 1894 [1].

Another individual who had a major impact on electricity and magnetism was Nikola Tesla. Born in 1856, Tesla began his studies in mechanical engineering, mathematics, and physics at a polytechnic institute in Graz. After studying in Graz, Tesla moved to Prague where he continued his studies. From Prague, Tesla moved to Budapest where he worked for telephone company. While in Budapest, in 1882, he invented AC power transfer and the induction motor. In 1884, he moved to the US and began working for the Edison Company in New York City. Tesla left his job working for Edison and, in 1885, formed the Tesla Electric Company. Between 1887 and 1888, Tesla used his business as a springboard to patent more than 30 inventions. Tesla was a relatively unknown name until 1888 when he gave

a lecture on his newly-developed AC power transfer system to the American Institute of Electrical Engineers (AIEE). After that pivotal lecture, Tesla became very famous. In 1889, Tesla partnered with George Westinghouse of the Westinghouse Company and transferred license of his multiphase current patents to them. Then, in 1895, Tesla and the Westinghouse Company built the first, full-scale, AC power transfer system at Niagara Falls. Toward the end of the 19th century, in 1891, Tesla gave another lecture to the AIEE during which he discussed his experiments with AC and their application in creating artificial lighting. This application would later become known as a "Tesla coil". During this lecture, Tesla also proposed a schema for using a condenser in series with a high-frequency alternator in the primary winding of a transformer. A large, insulated, metal plate was to be connected to the secondary winding. Another metal plate connected to an electric-powered light would allow for the light to be place anywhere within, or beyond, the plates. This assertion was crucial in that it was the first use of a transformer containing resonant circuits in a manner that suggests he was already thinking about wireless power transfer. In 1900, Tesla returned to New York after working in his Colorado Springs laboratory for a few years. At this time, Tesla built a new laboratory in Wardenclyffe, Long Island for developing and implementing a system for global wireless power transfer. He outfitted the laboratory with an enormous antenna for use in transmitting energy ranging from "minute amounts" to "amounts of industrial significance" [1]. Unfortunately, Tesla did not acquire the necessary investments to carry out the project and, after three years, gave up on his dream of providing the world with wireless power [1]. Tesla's research had a profound impact on a number of industries, but wireless power transfer did not obtain much exposure until 2006 when a team of MIT researchers rediscovered his findings on the subject.

In 2007, Aristeidis Karalis, John D. Joannopoulos, and Marin Soljačić wrote a paper on their research in efficient wireless non-radiative mid-range energy transfer. The triad was motivated by taking another look at Tesla's findings from the early part of the 20th century. While poring over his lab notes, they found detailed accounts of Tesla's attempts to transfer large amounts of energy over great distances with little luck. They determined that, even if Tesla has accomplished this feat, it would have been an ill-fated technology; Tesla's research was in radiative energy transfer using omnidirectional antennas. This schema would have resulted in a significant loss of energy to free space. The group also asserted that directed radiation was not plausible because it required a line-of-sight between the emitter and receiver. This, ultimately, led the team to the conclusion that mid-range power transfer is the most needed WPT schema today since power grids across the world carry power to nearly every corner of the civilized world. While analyzing the currently used schemata for

non-radiative WPT (magnetic induction in this case), Karalis et al. found that all were limited to incredibly low-power or close-range transfer. They investigated utilizing "long-lived oscillatory resonant electromagnetic modes, with localized slowly-evanescent field patterns, for efficient, wireless, non-radiative, mid-range energy transfer" based on the physical principle of resonant coupling [3]. Resonant coupling occurs when two like-frequency resonant objects couple and have minimal interactions with objects in the immediate vicinity that are off-resonant. This physical principle was well-established for near-field energy transfer, but had yet to be explored for mid-range energy transfer. Their paper showed that efficient, mid-range WPT can be accomplished via highly coupled magnetic resonance, which results in minimal dissipation of power into nearby off-resonant objects and free space. Karalis et al. proved that wireless power transfer at mid-range distances can be accomplished with a non-radiative schema by using the physical principle of resonance to allow strong coupling between objects while minimizing intrinsic losses [3]. This advance in the field of WPT has led to many more developments that will be discussed later in this paper.

From electric toothbrushes to tea kettles, WPT has been applied to a very diverse set of products. Many of those products accomplish WPT via electromagnetic induction or inductive coupling, a WPT schema that allows for very short range power transmission. Inductive coupling is accomplished when an alternating current runs through a primary coil, thereby creating an oscillating magnetic field, which, subsequently, induces a voltage on a nearby secondary coil [4]. This process is also how power is transferred between windings of a transformer [4]. The main difference between these two systems is the type of core to which the magnetic field is restrained [4]. In the former, the core consists of an air gap; the latter uses a core with high permeability to confine the oscillating magnetic field [4]. As the air gap increases between two coils, the efficiency of power transfer drops. This schema is great for smaller, less power-intensive devices, but fails when attempting to wirelessly power devices efficiently over distances of more than a few centimeters. A longer-distance WPT schema that has become more well-known as of late is electrodynamic induction or resonant inductive coupling. The addition of a capacitor in parallel with the secondary coil forms a circuit that resonates at the frequency of the voltage source that is driving the primary coil [4]. By establishing resonance between the primary and secondary coils, radiative losses are drastically reduced and transfer efficiency can reach 40%-50% [4], [5]. It has been proven, both theoretically and experimentally, that WPT via inductive coupling is only made practical through the introduction of resonance; without resonance in either the primary or secondary coil, the efficiency drops considerably [5]. By enabling strong resonant coupling between the receiver and transmitter, the transmission of 60 W over distances as great as 2 meters has

been recorded, albeit with close to 40% efficiency [5].

This schema is under constant development and many bright minds have contributed to advancements in the field of non-radiative WPT over the last several years. The technology has improved to a point where it is being considered for a variety of applications, ranging from charging electric car batteries to powering biomedical implants. As WPT becomes more widespread, and there is open access to ambient power anywhere (similar to Wi-Fi and the Internet), the need to implement controlled access arises. Assuming WPT is as pervasive as Wi-Fi, without controlled access any individual with a compatible device, such as a phone or laptop, could park himself outside a place of business and leach power from the WPT hub located within the business. Power theft is not a new concept; when electric vehicles were first outfitted with a standard 3 prong, 110 VAC plug, there were reports of individuals plugging their car into outlets on the sides of buildings on property they did not own [6]. A controlled access schema would prevent people from stealing power from a system that they are not authorized to access. A simple, proof-of-concept, gatekeeping schema could be implemented through the incorporation of three components: an incredibly isolated resonance frequency, multi-loop switching, and a random number generator that is seeded by a password. An isolated resonance frequency can be achieved through coil design, such that a slight detuning of the coil results in a near-zero power transfer efficiency. Multi-loop switching will enable the WPT hub to switch between a series of coils, each with a unique, isolated, resonance frequency. The hub will switch loops every time the internal clock ticks. Finally, the random sequence generator will provide the system with the sequence and duration of each loop switch. This random generator will be seeded by a password. If a user were to enter this password on his receiving circuit, he would be able to identify the loop-switching sequence, synchronize his receiver loop-switching sequence via a "stop bit", and connect to the hub.

While this system could be broken or cracked, it is a proof of concept that wireless power transfer, an analog system, can be encrypted in a quasi-digital manner similar to that of wireless networking. Therefore, the primary objective of this thesis is to explore how the shape, size, and dimensionality of the primary and secondary coils impacts the resonance frequency of the system. It is crucial to the development of a controlled access schema that resonance frequencies can be isolated. The coil design will be optimized experimentally, to verify the isolation of resonance frequencies, by developing a variety of coil types and structures and determining which design characteristics allow the loop to approach an isolated frequency. A secondary objective is the implementation of a multi-loop, switching mecha-

nism that will enable WPT from a variety of unique resonance frequencies. Finally, a tertiary objective is to incorporate a random sequence generator that can be seeded by a user-input password. The generator will develop a unique, loop-switching sequence such that a user can only draw power if his receiver device matches the sequence exactly. By accomplishing the aforementioned objectives, a simple wireless power transfer encryption system will have been proven. This research will lay the groundwork for more sophisticated WPT schemas that prevent the unauthorized transmission of wireless power.

Chapter 2

WPT Fundamentals and Current State-of-the-Art

2.1 WPT Fundamentals

As was described in the previous chapter, the WPT schema focused on in this thesis is strongly coupled magnetic resonance (SCMR). This schema is also referred to as resonant inductive coupling, electrodynamic coupling, and magnetic resonant coupling. Before expanding on the details of wireless power transfer using strongly coupled magnetic resonance, it is imperative to have a firm understanding of resonance. Kurs et al. cover the formalism of resonance using coupled-mode theory and, ultimately, derive the following equation:

$$\dot{a}_m(t) = (i\omega_m - \Gamma_m)a_m(t) + \sum_{n \neq m} i\kappa_{mn}a_n(t) + F_m(t) \tag{2.1}$$

In this equation, $a_m(t)$ is defined such that the total energy contained within object m is equal to $|a_m(t)|^2$. The resonant angular frequency of object m is represented as ω_m. The intrinsic decay due to radiated and absorbed losses is represented by Γ_m. The terms κ_{mn} and κ_{nm} are equivalent and represent the coupling coefficients between the resonant objects [5]. A pair of objects, source and device, identified by subscripts S and D, respectively, has a coupling coefficient, κ, that represents the strength of coupling. A load, represented by subscript W, acts as a resistance connected to the device and extracts work from it. This results in an overall intrinsic decay rate of $\Gamma'_D = \Gamma_D + \Gamma_W$. The total work extracted from the device by the load is calculated from the total power dissipated in the load, $2\Gamma_W|a_D|^2$.

Efficiency of the energy transfer is given by the following relationship:

$$\eta = \frac{\Gamma_W |a_D|^2}{\Gamma_S |a_S|^2 + (\Gamma_D + \Gamma_W)|a_D|^2} = \frac{\frac{\Gamma_W}{\Gamma_D}\frac{\kappa^2}{\Gamma_S \Gamma_D}}{[(1 + \frac{\Gamma_W}{\Gamma_D})\frac{\kappa^2}{\Gamma_S \Gamma_D}] + [(\Gamma_D + \Gamma_W)^2]} \tag{2.2}$$

Efficiency is maximized when the ratio of losses, $\frac{\Gamma_W}{\Gamma_D}$, is equal to $[1 + (\frac{\kappa^2}{\Gamma_S \Gamma_D})]^{\frac{1}{2}}$. Therefore, to develop an efficient power transfer schema, $(\frac{\kappa^2}{\Gamma_S \Gamma_D})$ must be greater than 1. A system that exhibits this efficient energy transfer is often referred to as strongly coupled [5].

In their publication, Kurs et al. outline a theoretical model to describe self-resonant coils. It should be noted that their theoretical work relies on coupled-mode theory. The coils are defined by their total length l, height h, and cross-sectional radius r. The effective capacitance C and effective inductance L can be defined using EM theory:

$$\frac{1}{C} = \frac{1}{4\pi\varepsilon_0 |q_0|^2} \iint d\mathbf{r}\, d\mathbf{r}' \frac{\rho(\mathbf{r})\rho(\mathbf{r}')}{|\mathbf{r} - \mathbf{r}'|} \tag{2.3}$$

$$L = \frac{\mu_0}{4\pi |I_0|^2} \iint d\mathbf{r}\, d\mathbf{r}' \frac{\mathbf{J}(\mathbf{r}) \cdot \mathbf{J}(\mathbf{r}')}{|\mathbf{r} - \mathbf{r}'|} \tag{2.4}$$

The energy within the coil is defined by the following relationship:

$$U = \frac{1}{2} L |I_0|^2 = \frac{1}{2C} |q_0|^2 \tag{2.5}$$

which then allows us to define the resonance frequency as follows:

$$f_0 = \frac{1}{2\pi\sqrt{LC}} \tag{2.6}$$

By defining the resonance frequency as such, the self-resonant coil can be treated as a standard oscillator with $a(t) = \sqrt{\frac{L}{2}} I_0(t)$. The radiation and ohmic resistances are defined by:

$$R_r = \sqrt{\frac{\mu_0}{\varepsilon_0}} \Big[\frac{\pi}{12} n^2 \Big(\frac{\omega r}{c} \Big)^4 + \frac{2}{3\pi^3} \Big(\frac{\omega h}{c} \Big)^2 \Big] \tag{2.7}$$

$$R_o = \sqrt{\frac{\mu_0 \omega}{2\sigma}} \frac{l}{4\pi a} \tag{2.8}$$

where n represents the number of turns in the coil and σ represents the conductivity of the coil. By knowing that the first term in Equation (2.7) is much larger than the second term, the coupled-mode theory decay constant for the self-resonant coil can be defined as

$\Gamma = \frac{R_o+R_r}{2L}$, with a quality factor of $Q = \frac{\omega}{2\Gamma}$. The power transferred to the source can be used to determine the coupling coefficient κ_{DS}:

$$\begin{aligned} P_{DS} &= \int d\mathbf{r}\mathbf{E}_S(\mathbf{r}) \cdot \mathbf{J}_D(\mathbf{r}) \\ &= \frac{1}{4\pi} \iint d\mathbf{r}\, d\mathbf{r}' \times \left[\mu_0 \frac{\mathbf{J}_S(\mathbf{r}')}{|\mathbf{r}' - \mathbf{r}|} + \frac{\rho_S(\mathbf{r}')}{\varepsilon_0} \frac{\mathbf{r}}{|\mathbf{r}\prime - \mathbf{r}|^3}\right] \cdot \mathbf{J}_D(\mathbf{r}') \\ &= -i\omega M I_S I_D \end{aligned} \tag{2.9}$$

From Equation (2.9) and the knowledge of coupled-mode theory, the following relationship can be concluded:

$$\kappa = \kappa_{DS} = \kappa_{SD} = \frac{\omega M}{2\sqrt{L_S L_D}} \tag{2.10}$$

In the above equations, it is clear that both κ and Γ are dependent on the frequency. This make it even more important to carefully design the coil size for a desired resonance frequency so as to optimize efficiency and, ultimately, transfer energy between the coils. It should also be noted that the coupling coefficient drops dramatically as the distance between the source and device coils increases [5]. Kurs et al. set out to experimentally prove the above theory. In their experiment, the group developed a scheme containing two self-resonant coils. The coils were helical and made of copper. The source coil, S, is inductively coupled with an alternating current circuit. The device coil, D, is inductively coupled with a resistive load [5]. This experimental setup can be seen in Figure 2.1.

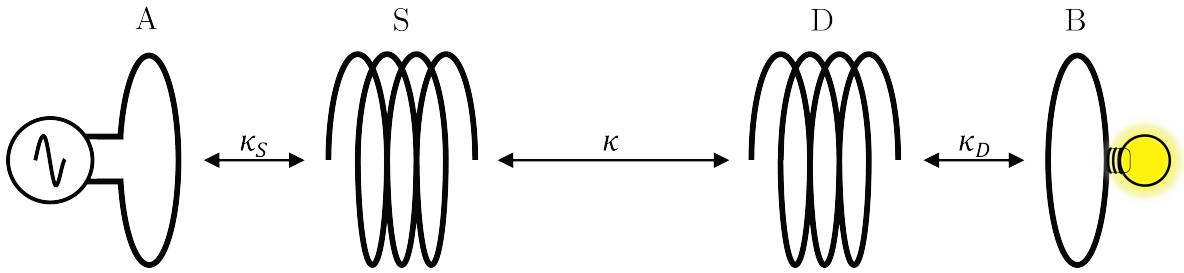

Figure 2.1: Experimental coil setup for strongly coupled energy transfer

The coils had height $h = 20$ cm, cross-sectional area $a = 3$ mm, and total number of turns $n = 5.25$. The loop spacing in the helical coils was not uniform and, to account for this uncertainty, an error margin of $\pm 10\%$ was applied to the height. The resonance frequency was calculated to be $f_0 = 10.56 \pm 0.3$ MHz, based on these coil parameters. The experimentally determined resonance frequency was 9.90 MHz. The circuit in Figure 2.1 successfully illuminated a 60 W light bulb at distances greater than 2 meters [5]. The results of the experiment can be seen in Figure 2.2.

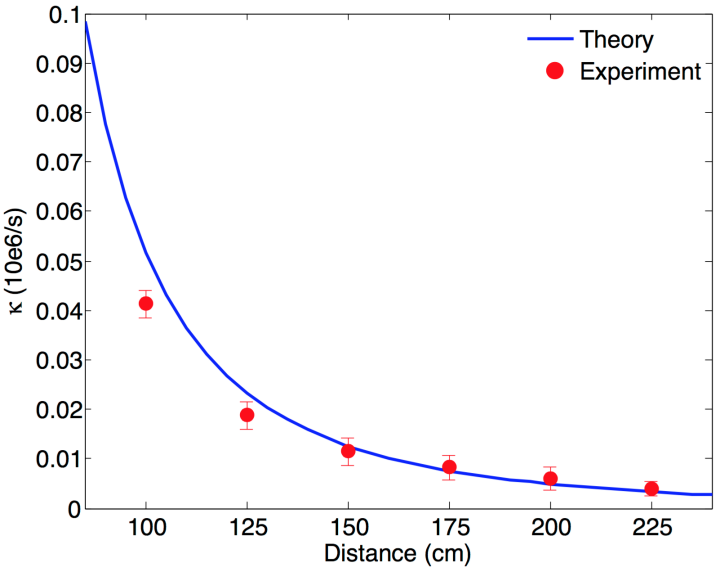

Figure 2.2: Theoretical and experimental results showing the relationship between coupling coefficient κ and distance between source and device coils when coils are coplanar, From [5]. Reprinted with permission from AAAS.

The theoretical research and experimentation completed by Kurs et al. provides a very thorough précis on wireless power transfer. The schema modeled by the group has enabled a great many developments in WPT, specifically in utilizing SCMR.

2.2 Prior Research

The research described in the previous section is the groundwork on top of which a variety of new discoveries have been made in the field of mid-range non-radiative wireless power transfer. Shortly after publishing their initial work on WPT via SCMR, Kurs et al. began researching ways to extend the transfer distance of their WPT schema. In their 2009 publication, Hamam et al. outline the concept of resonant repeaters. They proposed an efficient, yet minimally radiative, energy transfer system in which two self-resonant objects are strongly coupled with an intermediate object that has a matching resonance frequency. By matching the resonance frequency of all three objects, the system maintains high efficiency and the distance between the source and device coil can be expanded greatly. The inspiration for this distance-increasing feat was a quantum interference phenomenon called electromagnetically induced transparency (EIT). In EIT, three atomic states, one lossy and two lossless, are coupled. While this intuitively sounds as though it would create a lossy system overall, the opposite is true; by very carefully controlling the coupling between each coil, a system that

is non-lossy overall can be established. Physically, this can be demonstrated with a laser pulse, sent from the probe laser, directed at an incredibly opaque medium, which can be made transparent by sending the original laser pulse through an additional laser pulse, sent from Stokes laser. This is accomplished only with properly chosen temporal overlap between the two pulses. The functionality of resonant repeaters is considered EIT-like due to its similarity to this physical phenomenon. Interestingly, the use of resonant repeaters can enable more efficient and less-radiative transfer than the direct source-to-device coil energy transfer outlined in the previous section [7]. The incorporation of resonant repeaters into a WPT system not only makes the system safer for human interaction, due to the further-diminished radiation exposure, but also brings the concept of ubiquitous power closer to reality.

One of the first areas that was looked into, after Hamam et al. published their work, was the transfer of power from one source coil to multiple receiver coils of different dimensions. In mid-2009, Cannon et al. published a paper on a multicast system of sorts for WPT. They assert that a WPT system via SCMR does not require all coils in the system to be identical for the system to function efficiently. The property of the coils that is crucial to the WPT system is the resonance frequency. The resonance frequency of each coil in the system can be matched by choosing different lumped capacitances, as is shown in the following relationship:

$$\omega_0 = \frac{1}{\sqrt{L_S C_S}} = \frac{1}{\sqrt{L_D C_D}} \tag{2.11}$$

It is clear from Equation (2.11) that, by adjusting the capacitances or inductances of the coils, a common resonance frequency for both source and device coils can be achieved. The group theoretically and experimentally verified this assertion. In doing so, they identified an issue that occurs in multiple-receiver energy transfer systems: frequency splitting. This phenomenon occurs when receiver coils are close enough to one another that the two receivers experience strong coupling between their magnetic fields. This issue can be mitigated by adding control circuitry to the WPT system that identifies shifts in resonance frequency and adjusts the receiver coil capacitances, resulting in changes to the resonance frequencies of the coils [4].

In 2010, a group from the University of Tokyo published a paper on improving the efficiency of a SCMR WPT system via impedance matching. Beh et al. opted to avoid using coupled-mode theory to describe the schema; instead, they used antenna and circuit design theories. The group first distilled the wireless power transfer system, outlined in the previous section, down to an equivalent circuit. This circuit can be seen in Figure 2.3.

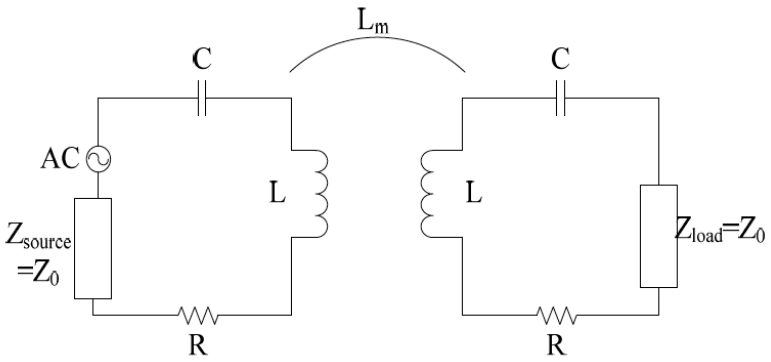

Figure 2.3: Equivalent circuit of wireless power transfer system [8]

Using circuit theory, the power transfer efficiency and coupling coefficient relationships were determined:

$$\omega_m = \frac{\omega_0}{\sqrt{1+\kappa}} = \frac{1}{\sqrt{(L+L_m)C}} \tag{2.12}$$

$$\omega_e = \frac{\omega_0}{\sqrt{1-\kappa}} = \frac{1}{\sqrt{(L-L_m)C}} \tag{2.13}$$

$$\kappa = \frac{L_m}{L} = \frac{\omega_e^2 - \omega_m^2}{\omega_e^2 + \omega_m^2} \tag{2.14}$$

$$\eta_{11} = S_{11}^2 \tag{2.15}$$

$$\eta_{21} = S_{21}^2 \tag{2.16}$$

$$S_{21}(\omega) = \frac{2jL_m Z_0 \omega}{L_m^2\omega^2 + \left[(Z_0+R) + j(\omega L - \frac{1}{\omega C})\right]^2} \tag{2.17}$$

In these relationships η_{11} is the ratio of power reflection, η_{21} is the ratio of power transmission, S_{11} is the reflected wave ratio, and S_{21} is the transmitted wave ratio. It was found that the resonance frequency of the coils changes as the coupling coefficient between the coils changes. To prevent this from happening, and to allow continuous coupling with the source coil, an impedance matching circuit can be introduced. This technique is often used in communication systems and power transfer systems to improve efficiency. The impedance matching circuit minimizes the power reflection back to the source, which improves the efficiency of the system. It should be noted that, if the resonance frequency of the system is already matched to the power source frequency, the efficiency of the system cannot be further improved. Ultimately, impedance matching allows for the resonance frequency of WPT system to adhere to the frequency of the power source. Without a mechanism to ensure a constant, common, resonance frequency, the system could encroach on frequency bands that

are off limits. This is particularly important for the future standardization of WPT; there are many regulations that govern the use of frequency ranges in communications and power transfer, and it is often necessary to remain within a particular frequency band to comply with said regulations [8].

Imura and Hori, two authors of the previously mentioned publication, produced another work in 2011 that showed that the use of the equivalent circuit for a WPT system and the Neumann formula could maximize efficiency and the distance between coils. It was found, using the Neumann formula, that the distance between coils is related to the number of turns and radius of the coils. Therefore, maximum efficiency at a specified distance between coils can be achieved by adjusting four variables: resonance frequency ω_0, characteristic impedance Z_0 (due to the circuits connected to the coils), internal resistance of the coils R, and mutual inductance between the coils L_m. This work enables optimization of WPT system design to improve overall system efficiency [9].

Another major advancement in wireless power transfer via SCMR came in 2011 with the publication of a Master's thesis on WPT for industrial applications. In the thesis, Pannier et al. redesigned the coils to improve transfer efficiency. Four types of coils were tested: solenoid, rectangular, planar circular, and planar square. Each type of coil was determined to have an optimal distance from the source coil. This distance is the point at which maximum transfer efficiency occurs. The rectangular and solenoid coils had an optimal distance of less than 5 mm. The planar coils had an optimal distance of approximately 20 mm. It should be noted that this research did not use any of the previously mentioned techniques to improve efficiency, coil distance, or coupling coefficient. While holding the distance between coils constant, each type of coil was angularly displaced to evaluate how rotation of a coil affects the efficiency of the power transfer system. The planar coil types fared much better in this test; they boasted efficiencies up to 25% higher than the other two types of coils. This test also showed that an increase in angular displacement linearly decreases the efficiency of the power transfer system. This information is very useful for the future of coil design; the determination that planar coils perform better at greater distances, and are less impacted by angular displacement, leads to the conclusion that future WPT systems can be easily adapted to and included in printed circuit board (PCB) designs [10]. It has since been suggested that the geometry of planar coil design could also be explored so as to find a shape for a planar coil that optimizes transfer efficiency [11].

In 2011, Duong and Lee published their research on using a variable coupling method to

transfer power wirelessly, rather than the traditional fixed coupling method that has been used in the previously mentioned studies. The technique of variable coupling enables higher efficiency as the distance between source and device coils is varied. This is accomplished by altering the coupling coefficient between the power source and the source coil. Using Figure 2.1 as a reference, due to the symmetry of the system, it can be deduced that the coupling coefficient κ_{AS} between the power source coil A and the source coil S is equal to the coupling coefficient κ_{DB} between the device coil D and receiver coil B. The quality factor of each coil in the system is defined by Q_i, where i designates the letter corresponding to the coil (i.e. A, S, D, B). The symmetry of the system ensures that $Q_A = Q_B$ and $Q_S = Q_D$. Based on these determinations, the following equation holds true:

$$\kappa_{AS}^2 = \frac{\sqrt{\kappa_{SD}^2 Q_S + 1}}{Q_A Q_S} \tag{2.18}$$

Empirically, when the distance between coils increases, there is a corresponding decrease in the coupling coefficient between the two coils. It is clear from Equation (2.18) that, to maintain the coupling coefficient κ_{SD} between the source coil and the device coil, either Q_A or κ_{AS} must be decreased. Duong and Lee experimentally verified this relationship and used the variable coupling method to allow for increased efficiencies at greater distances. Variable coupling was accomplished by varying the distance between the power source coil and the source coil, concurrently with distance between the device coil and receiver coil. In other words, if the distance between the source coil and device coil increases, the coupling coefficient κ_{SD} between the two coils drops, resulting in a reduced efficiency. To combat this reduction in efficiency, the coupling coefficient κ_{AS} between the power source coil A and source coil S is increased by decreasing the distance between them. Due to the necessity of symmetry in the system, the distance between device coil D and receiver coil B is decreased as well. The results of this method can be seen in Figure 2.4 [12].

It is apparent from Figure 2.4 that these adjustments result in a constant coupling coefficient between the source and device coils, which allows for higher efficiency between the two coils at larger distances [12].

By mid-2012, wireless power transfer had begun to take hold outside of academia. A triad of Qualcomm Incorporated employees published a paper on loosely-coupled wireless power transfer (LC WPT). In this work, Grajski, Tseng, and Wheatley envision a world without wires, particularly from a consumer electronics standpoint. This feat, they assert, will be accomplished via LC WPT. They define LC WPT as a resonant wireless power transfer system

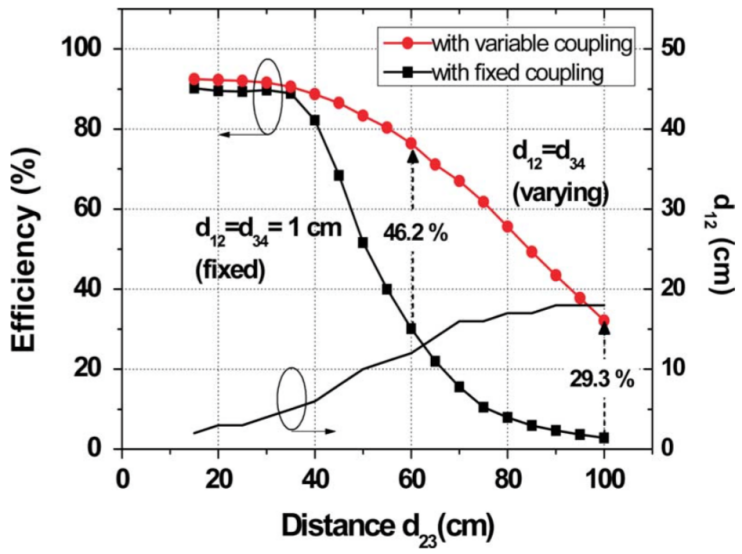

Figure 2.4: Comparison of WPT systems utilizing fixed and variable coupling [12] ©2011 IEEE

in which coils are so loosely coupled that their coupling coefficients can be less than 0.1, but can also be as high as 1, while still transferring power. To embrace such a system, the group maintains that it is crucial for LC WPT to be properly categorized and appropriately regulated. The suggested frequency bands for WPT are the Industrial, Scientific, and Medical (ISM) bands, which are defined by the International Telecommunication Union Radiocommunication Sector (ITU-R). These bands are suggested because of their lack of restrictions on emissions. Grajski, Tseng, and Wheatley conclude their paper with the declaration that, in order to make ubiquitous wireless power a reality, LC WPT must be integrated in such a way that it works well with currently existing systems and shows complete compliance with all applicable regulations [13]. The publication of this paper by a non-academic institution, in particular one that specializes in consumer electronics, illustrates that wireless power transfer is moving from concept to reality, giving additional credibility to future research and initiatives in the field.

In 2013, the concept of loop switching was evaluated by a group of researchers in South Korea. The authors, Kim, Choi, and Jeong propose a loop switching method to improve upon the efficiency of WPT systems. This schema utilizes multiple loops of varying sizes that are controlled using a switching device. By switching between loops at the power source and receiver, the system can adjust the coupling coefficient dynamically to allow for a more efficient transfer. The proposed system can be seen in Figure 2.5.

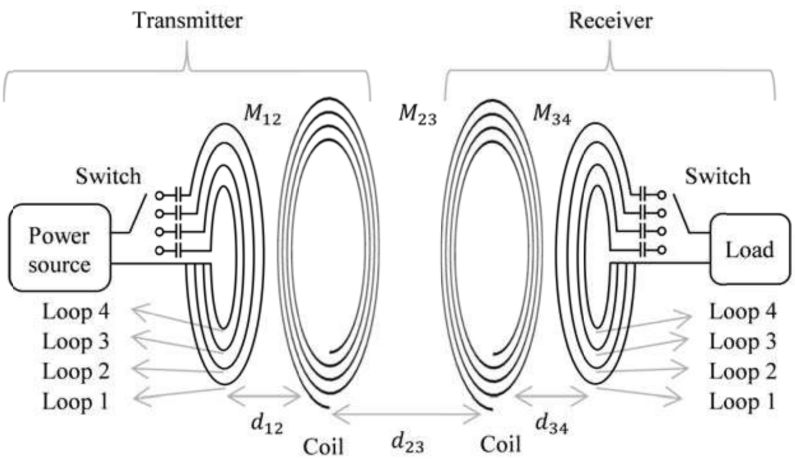

Figure 2.5: Loop switching WPT system, reproduced courtesy of The Electromagnetics Academy [14]

The method of loop switching to improve efficiency is similar to those discussed earlier in this chapter. As the distance d_{23} is increased, the efficiency of power transfer drops. The system detects this drop in efficiency, switches to a smaller coil, and high-efficiency power transfer is restored. Kim, Choi, and Jeong completed both simulation and experimentation to verify that the proposed method maintains high efficiency as the distance d_{23} is increased. The results of their study can be seen in Figure 2.6.

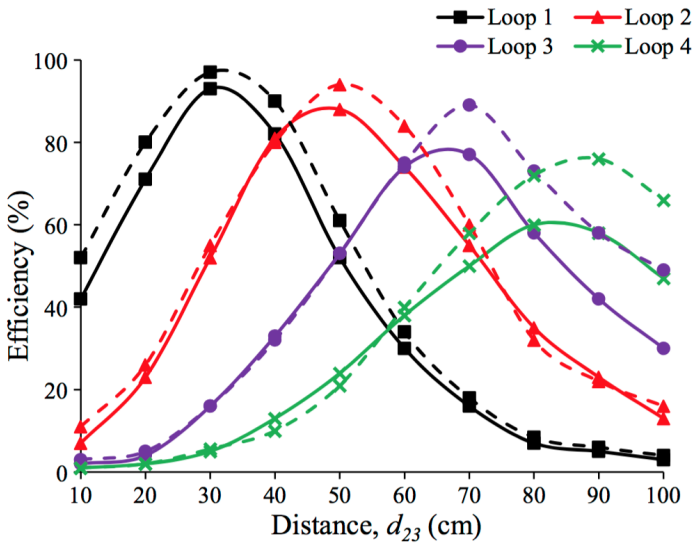

Figure 2.6: Loop switching simulation (solid) and experimentation (dashed) results, reproduced courtesy of The Electromagnetics Academy [14]

The figure above illustrates how dramatically this loop switching method improves the power

transfer efficiency as the distance d_{23} increases. By adding more loops to the system, an efficiency could be generally maintained, preventing the sudden drops in efficiency that can be seen in the four-loop, switching system [14].

All of these advancements in the field have further proven that WPT via SCMR is a viable means of mid-range, non-radiative, power transfer. The improvements in transfer efficiency invalidate any claims that WPT is far too inefficient to be economical. The developments made in maximizing efficiency while increasing distance allow for a more comprehensible vision of ubiquitous power. Additionally, the publication of a paper by a consumer electronics company illustrates that the industry views WPT as an emerging technology. The call for standards and regulation of the technology show that a concerted effort is being made to ensure the establishment of a standard WPT protocol, similar to how wireless communication is standardized and regulated currently. Finally, variable coupling and loop switching provide a means for maintaining highly-efficient power transfer, even as distances increase. Collectively, these improvements signify that WPT is ready to be adopted by consumers, and supported by companies and industries, across the globe. These advancements have set the stage for a world without wires; one in which ubiquitous wireless power enables constant charging, refueling, and powering of all of our most coveted devices.

Chapter 3

Simulation Study and Motivation for Experimental Analysis

In January 2014, we began exploring WPT via SCMR using an experimental setup, modeled after the setup from the paper by Kurs et al., in Miami University's EM laboratory. The WPT system very closely matched the design in Figure 2.1. Pictures of the system can be seen in Figure 3.1 and Figure 3.2.

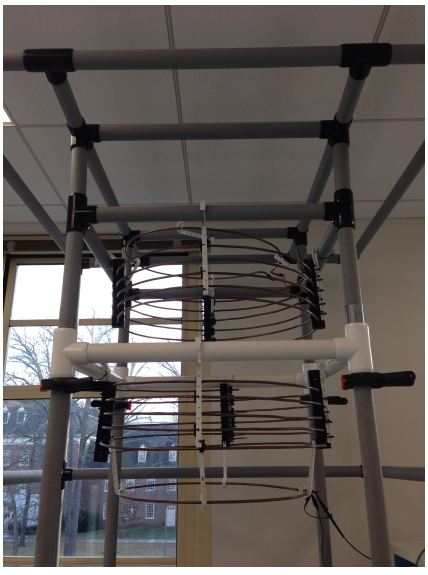

Figure 3.1: Front view of experimental WPT system

Figure 3.2: Bottom view of experimental WPT System

This setup was constructed for a senior capstone project in 2008, after the team had learned of the work of Kurs et al. into WPT. From January through May, after exploring the labo-

ratory setup and becoming acquainted with basic WPT, we collated relevant research in the field of WPT via SCMR. Perhaps the most important research we reviewed related this thesis was the utilization of resonant repeaters to allow for greater distance and permeation of WPT. Resonant repeaters allow power to be distributed so ubiquitously that someone could feasibly be outside of a building and "tap in" to the power source. By September 2014, this literature review had led us to identify a unique problem that had not yet been addressed: pervasive WPT would enable an unauthorized individual to leech power from a WPT system.

Between September and November, we began formulating different methods by which we could prevent an unauthorized individual from accessing a power source wirelessly. In doing so, we naturally related the system to a protected local area network (LAN) that is accessed via Wi-Fi. The prominent difference between the two systems is that Wi-Fi is inherently digital, whereas WPT via SCMR is strictly analog. We began to look into the concept of resonance frequency switching in such a way so as to prevent unauthorized users from accessing it. For this to be a feasible gatekeeping mechanism, the resonance frequencies that the system switches between must be disparate enough for a device to receive no power, or negligible power, if it is not tuned to the proper resonance frequency.

In November 2014, we decided on an approach to determine the characteristics that allow for isolated resonance frequencies: simulate our laboratory's proven experimental WPT system through software to verify the validity of the simulation results. After verifying the capability of the software, we would adjust the coil design to hone in on isolated resonance frequencies. In December 2014, we came across a set of white pages published by Ansys on WPT simulation in their High Frequency Structural Simulator (HFSS). This tool is often used for complex antenna and RF circuit design, but the document confirmed that the tool could also be used for our purposes. In our effort to recreate the lab setup, the WPT system proved far too large to effectively simulate in HFSS. Instead, we chose to recreate setups from experiments documented in papers published on WPT. These documented results, compared with those of an identical, simulated setup, would still enable us to verify that HFSS simulates physical WPT systems properly. Following verification, we would then optimize coil design to isolate resonance frequencies. After our thorough literature review, we decided that this isolation would be accomplished by simulating a coil with variations in the following parameters: coil size (i.e. radius for circular coils or length and width for rectangular coils), distance between coils, coil material, coil shape, and coil cross-sectional area. After simulating, we planned to take the high-efficiency variations and complete a few different laboratory experiments on variants of those to further optimize the isolation of

resonance frequencies.

In early February 2015, we modeled our first coil in HFSS. An image of the copper loop can be seen in Figure 3.3 below.

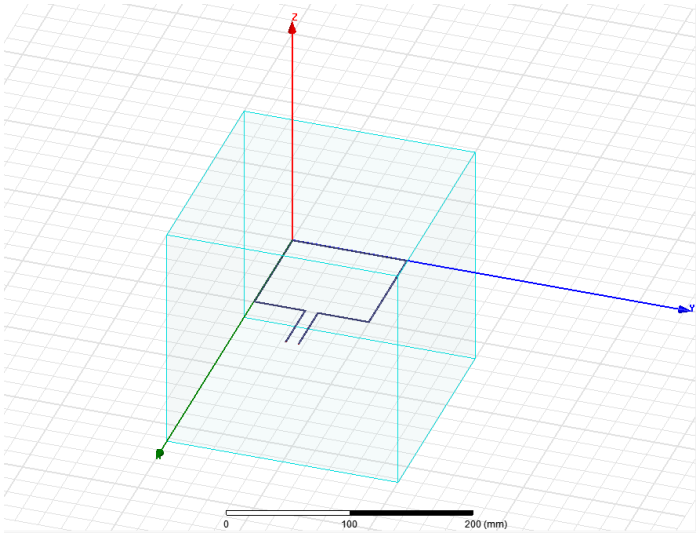

Figure 3.3: Planar coil designed in HFSS

The coil was designed to be planar, so as to be easily adapted to a PCB design. An aerial view of the coil can be seen in Figure 3.4. In this diagram, W is equal to 1 mm, the width of the coil trace. The thickness of the coil trace was set to 0.1 mm, to simulate the thickness of a trace on a PCB.

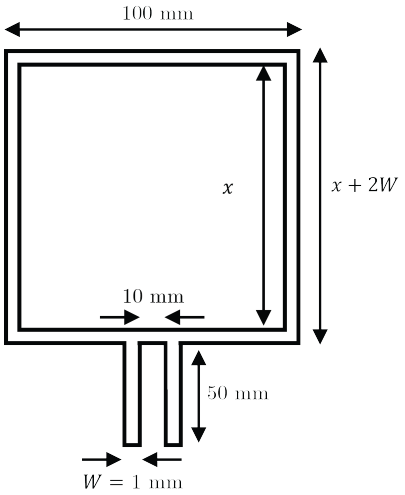

Figure 3.4: Diagram of a single coil (not to scale)

In this diagram, x represents coil length, from internal edge to internal edge; it ranged from

10 mm to 100 mm by increments of 10 mm. All of the coil design parameters are given in Table 3.1.

Parameter	**Dimension (mm)**
Trace thickness	0.1
Coil width (outer edge to outer edge)	100
Coil length (outer edge to outer edge)	102
Lead length	50
Lead spacing (inner edge to inner edge)	10
Trace width	1

Table 3.1: Coil design parameters

The design outlined above was simulated from 1 MHz to 20 GHz for a one-coil system (see Figure 3.3) where $x = 100$ mm. By using a one-coil system, the simulation yielded the reflection coefficient of the loop. The results of this simulation can be seen in Figure 3.5. In this plot, it is clear that the reflection coefficient is minimized at 13 GHz. Therefore, if we were to send that frequency to the loop, we can expect to minimize reflection loss as the EM wave propagates into space.

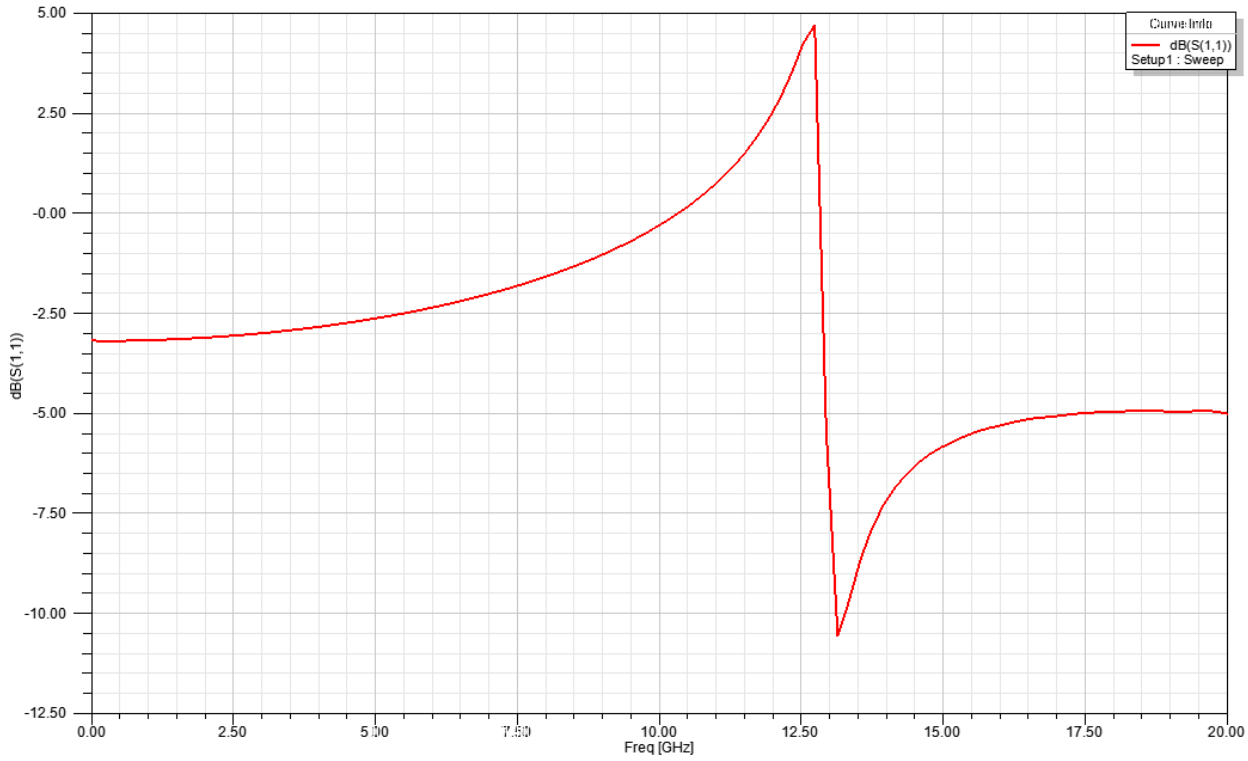

Figure 3.5: Reflection coefficient of a single coil

The coil was then duplicated and spaced 50 mm from the original coil. The 3D model of

this setup is shown in Figure 3.6. The simulation was run again, with frequencies ranging from 1 MHz to 20 GHz; both of the coils were identical and had the same parameters, as in the previous simulation.

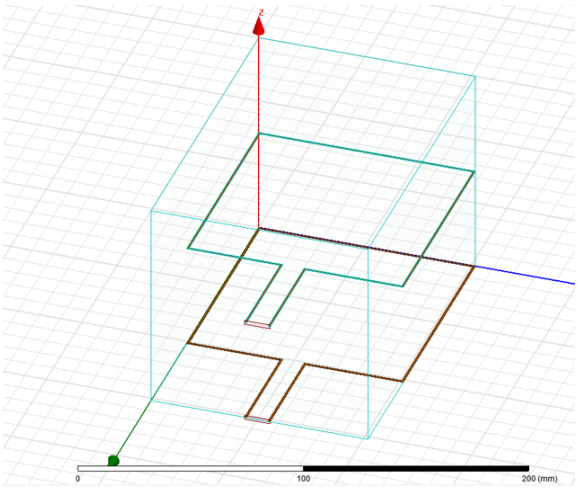

Figure 3.6: Two identical coils spaced 50 mm apart

The plot in Figure 3.7 shows the magnitude of the s-parameter for the system. The s-parameter or scattering parameter allows us to see how energy transfer between coils changes as the frequency changes.

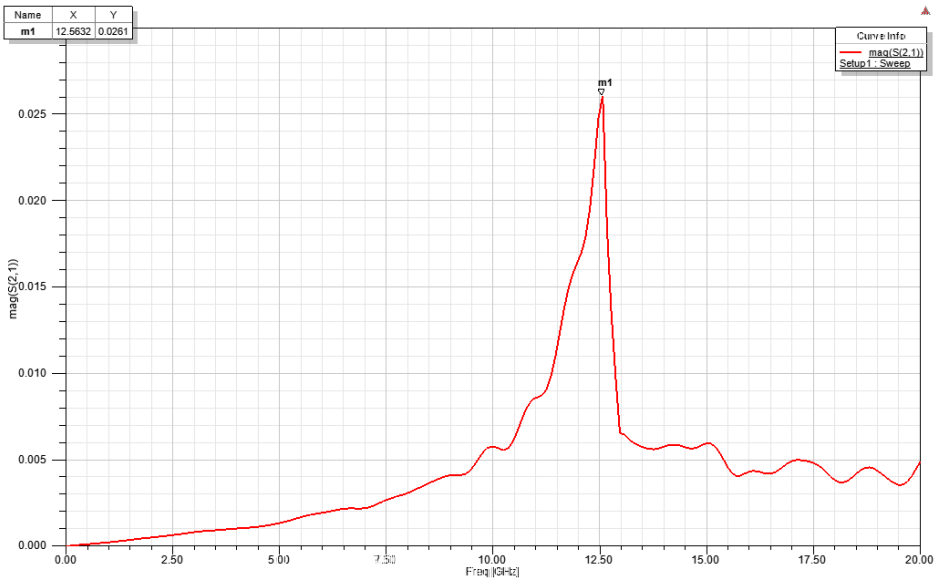

Figure 3.7: Magnitude of the S-parameter as frequency ranges from 1 MHz to 20 GHz

This plot shows that the maximum energy transfer between the coils occurs at 12.56 GHz, which tells us that is the resonance frequency of both coils since they are identical. A system in resonance minimizes losses to objects in the environment that are off-resonant, thereby

maximizing energy transfer between the resonant objects. This simulation was repeated for coil lengths from 10 mm to 100 mm in increments of 10 mm. The dependence of resonance frequency on coil length is shown in Figure 3.8.

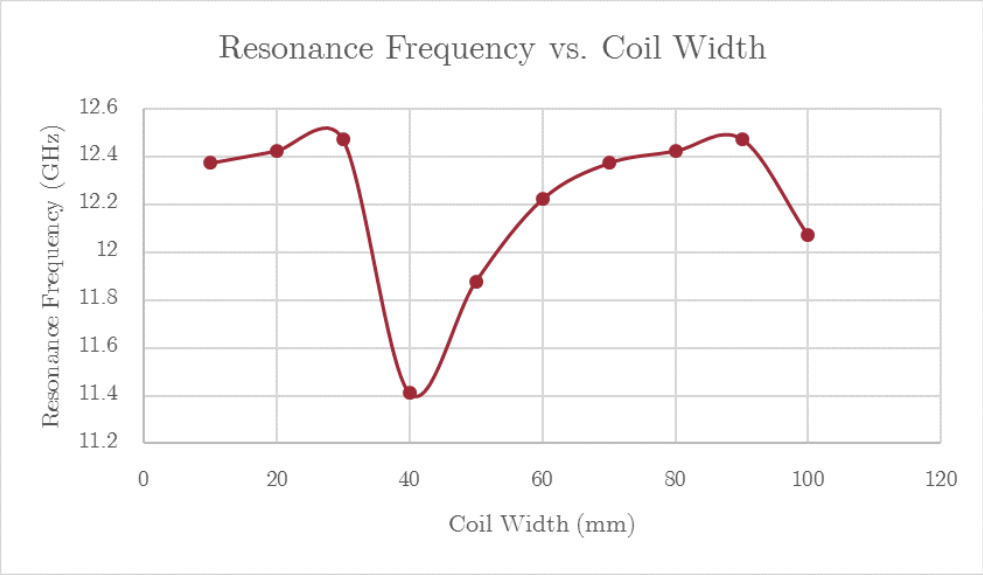

Figure 3.8: Dependence of resonance frequency on coil length

Due to the rectangular form of these coils, the resonance frequency does not change linearly, as it does with a circular coil. However, the drop in resonance frequency between the coil lengths of 30 mm and 40 mm is nearly 1.2 GHz, which led us to believe that there was an error inherent in the assumptions of our simulation. In an effort to determine how HFSS runs its simulation, using Ansys's Designer software, we created a circuit that was connected to a single coil to model the voltage of a step source over time. This circuit can be seen in Figure 3.9.

In the previous HFSS simulation, we had not specifically set a waveport impedance; it was set to a default value in the software. We opted to set the impedance of the waveport in HFSS to a value close to zero ($1\mu\Omega$) so that we could insert a 50Ω resistor in Designer. This allowed the impedance of the circuit to be fixed and independent of the waveport. This experiment enabled us to see how HFSS treats port impedance. The plot of the voltage over time can be seen in Figure 3.10. The lattice diagram contains an overshoot and undershoot on the rising edge of the step waveform because the coil's input impedance was not equal to the source impedance (50Ω).

Using the value of V_{in} from Figure 3.10, and the relationship $V_{in} = V_0 \frac{Z_c}{Z_c+Z_s}$, where $V_0 = 1V$ is the step voltage and $Z_s = 50\Omega$ is the source impedance, the coil impedance Z_c can be calculated. The calculated values for Z_c are listed in Table 3.2.

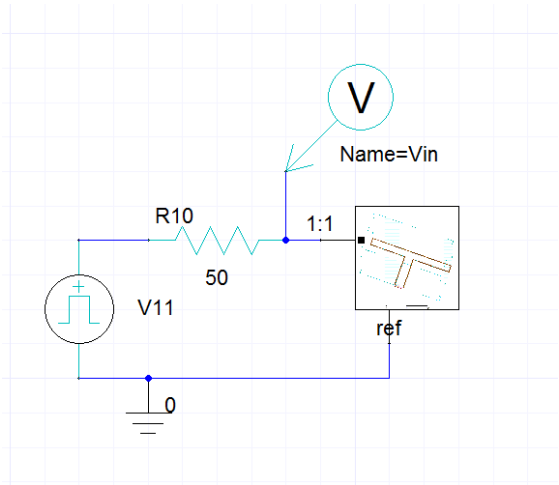

Figure 3.9: Circuit diagram for the source coil

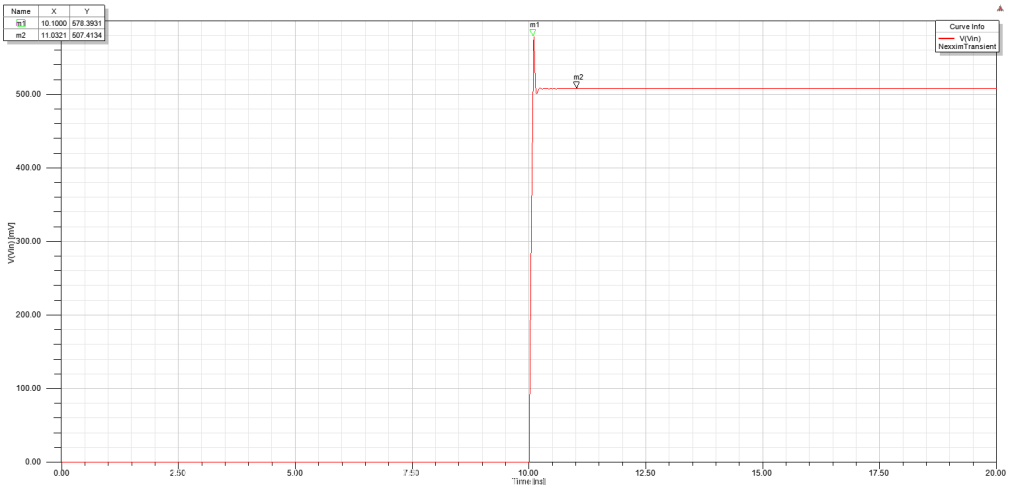

Figure 3.10: Lattice diagram showing the overshoot and undershoot due to mismatched impedances

As the coil impedance is very likely dominated by the inductive reactance, $j\omega L$, the lattice diagram approach is fallible. This fallibility is clear from the plots in Figure 3.11 and Figure 3.12. These plots show the magnitude of the s-parameter varying over frequency for the 10 mm and 100 mm coils, once they have been impedance matched with the Z_c values from Table 3.2.

Although the simulations using HFSS and Designer did not prove incredibly useful, they allowed us to determine a new course of action for our research. We decided that, given the ease of fabrication for PCBs today, and the ability to measure impedance in a lab using impedance meter, it would be best to proceed with our research through physical experimentation. This decision does not close the door completely on Ansys's HFSS and

Coil Length (mm)	V_0 **(V)**	V_{in} **(V)**	Z_0 **(Ω)**	Z_c **(Ω)**
10	1	0.43507	50	38.50654
20	1	0.43261	50	38.12281
30	1	0.43496	50	38.48931
40	1	0.43613	50	38.67292
50	1	0.43747	50	38.88415
60	1	0.43926	50	39.16789
70	1	0.43879	50	39.09321
80	1	0.43979	50	39.25224
90	1	0.43997	50	39.28093
100	1	0.43821	50	39.00123

Table 3.2: Calculated coil impedances that allow for proper impedance matching

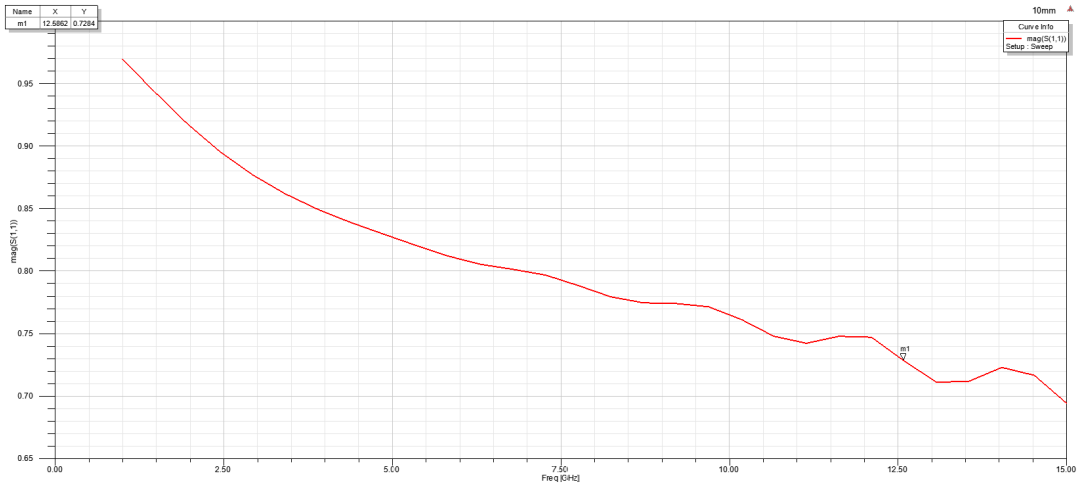

Figure 3.11: Magnitude of the S-parameter for a 10 mm length coil that has been impedance matched

Designer tools; we plan to use these tools to simulate our experimental laboratory setups as they progress. Therefore, we can use the experimental results to corroborate the results received from the simulations and determine whether HFSS and Designer are effective tools for simulating the design of our WPT system.

3.1 Final Approach

The objective of our thesis is to create a proof-of-concept WPT encryption system that prevents unwarranted access to the power source. This will be accomplished by establishing the relationship between coil design and resonance frequency, so as to isolate resonance frequencies for use in a coil-switching system. Four coils will be incorporated into the coil-switching

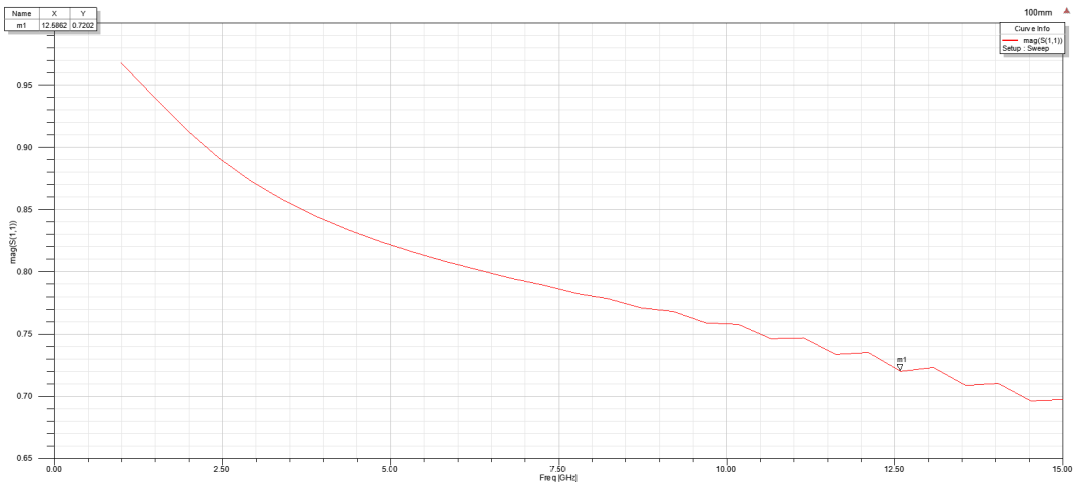

Figure 3.12: Magnitude of the S-parameter for a 100 mm length coil that has been impedance matched

system. These coils will be designed on printed circuit boards and will vary in size to yield a unique inductance for each coil. With each coil maintaining an identical capacitance and a unique inductance, unique resonance frequencies will be established. Impedance matching will be used to help isolate the resonance frequencies of the coils. We will be using a keypad to take user input and a linear feedback shift register (LFSR) to generate a random sequence. The input from the keypad will "seed" the random sequence generator. This allows the user input to act as a passcode. The sequence will be interpreted by a microcontroller unit (MCU) and the MCU will handle sending an enable signal to a designated relay, based on the sequence it has interpreted. The relay, when enabled, will switch the voltage source to the relay's corresponding power transmission coil. This system is illustrated in Figure 3.13.

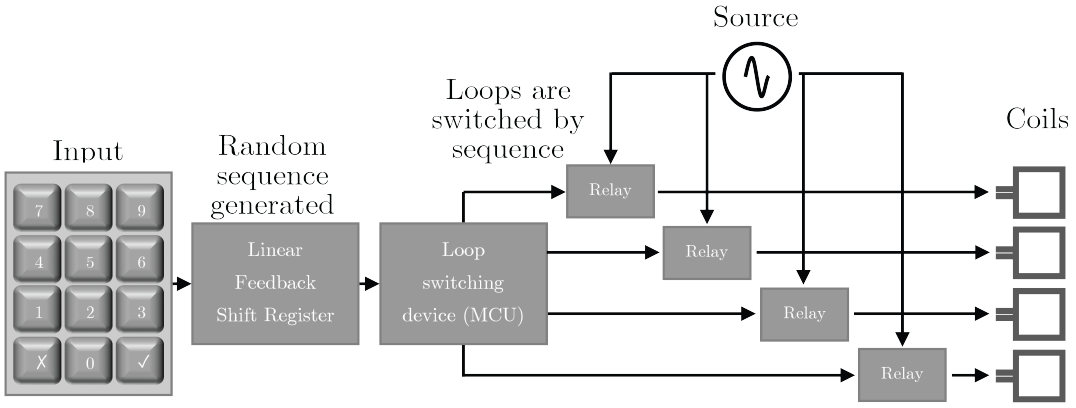

Figure 3.13: WPT controlled access system; TX

In the receiver (RX) circuit, there will be a set of four coils that are identical to those in the transmitter (TX) circuit. The coils will receive power via SCMR. A user who wishes to connect to the power source being transmitted will need to input the same passcode into the linear feedback shift register via the keypad on the receiving side. This passcode will allow the LFSR integrated circuit (IC) to be seeded in a manner identical to the transmitter. The MCU on the receiver side will handle synchronizing the receiver's switching sequence with the transmitter's switching sequence. Once the two sequences have been aligned, the device will be able to receive power from the transmitter. The receiver of the controlled access system can be seen in Figure 3.14.

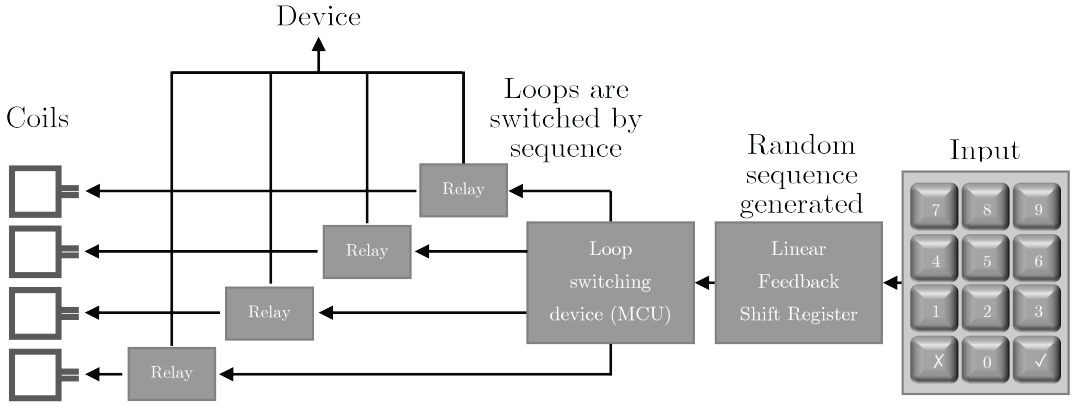

Figure 3.14: WPT controlled access system; RX

An unauthorized user will not be able to receive steady-state power because of the switching sequence. Since most WPT system only include one coil, the unauthorized user would, at most, be able to connect to the power source 25% of the time. To develop a more robust controlled access system, the four coils could be consolidated into one coil that has a

variable inductance, controlled by the MCU. This would allow the MCU to switch to nearly any resonance frequency (constrained by inductor range). By using a one-coil system with a large number of resonance frequencies, the system would become much more difficult to crack. Additionally, a one-coil unauthorized user would only be able to receive power when his coil's resonance frequency matches that of the transmitter, which becomes an increasingly smaller period as the number of resonance frequencies that are utilized increases. By proving the concept of controlled access for wireless power transfer systems, we will be further protecting the future of ubiquitous wireless power from those looking to abuse the system.

3.2 Final Goals

- Identify and utilize design considerations that isolate the resonance frequencies of the coils (50%)
- Integrate a circuit-based, loop-switching technique to enable continuous wireless power transmission while maintaining high efficiency (20%)
- Develop and implement a simple WPT encryption system using a numeric keypad and a four-digit code to authenticate the device with the source (30%)

Chapter 4

Experimental Analysis and Frequency-Selective Design Implementation

4.1 WPT via SCMR

Following our unsuccessful attempts to simulate WPT via SCMR in software, we set out to experimentally prove the concept of WPT encryption. The first step we undertook was experimental verification of WPT via SCMR. Using a function generator and two identical LC circuits for both the transmitter and receiver portions of the system, we successfully illuminated an LED that was connected in parallel with the receiver coil. A schematic of this basic WPT setup can be seen in Figure 4.1. There have been several papers documenting this procedure, but we wanted to ensure that we were building our encryption system on a WPT system that we knew to be functional, prior to adding any layers of security.

4.2 Receiver Frequency Switching

4.2.1 Axial Inductors in Series

After successfully demonstrating resonant wireless power transfer, we began looking into how to switch the resonant frequency of the WPT system. In many WPT studies, the inductance of the system, which contributes to the resonant frequency via the relationship

$f_0 = \frac{1}{2\pi\sqrt{LC}}$, is established through strategic design of the transmitter and receiver coils. By creating a coil with specific parameters, the inductance of the coil changes, resulting in a changed resonant frequency. We decided to look into using through-hole axial inductors in series with a single-loop coil. The small single-loop coil provides minimal inductance ($0.7\mu H$ in our case), but the axial inductor adds the remaining inductance needed to achieve our desired resonant frequency. An image of the experimental verification of this approach can be seen in Figure 4.2.

4.2.2 Axial Inductor in Parallel

Using axial inductors to achieve a specified resonant frequency opened the door to the idea of variable inductance within a WPT system. Inductors in series are additive, but inductors in parallel diminish the equivalent inductance, as is shown in Equation 4.1.

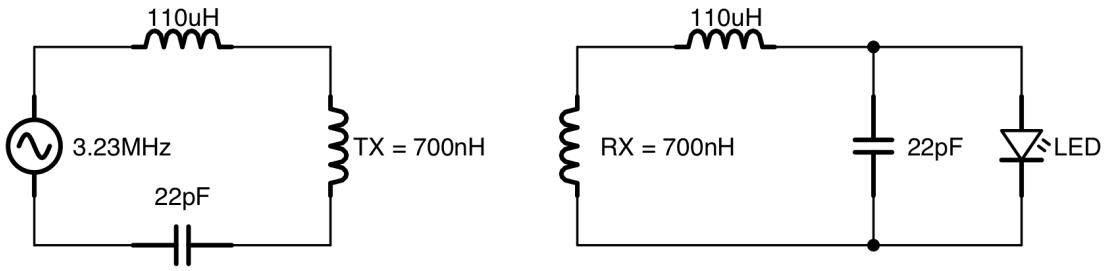

Figure 4.1: Schematic of a simple WPT system

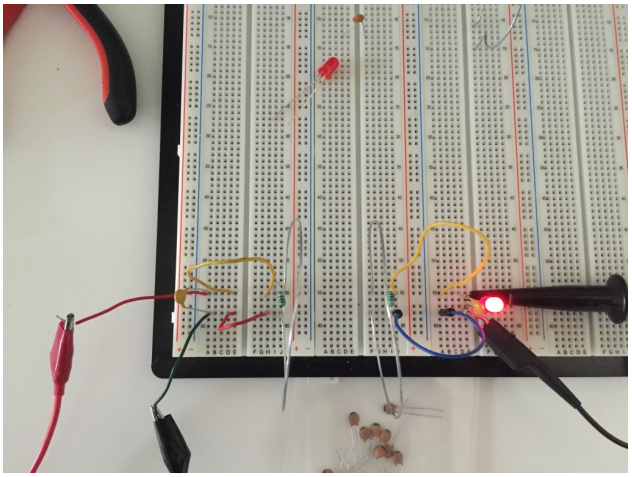

Figure 4.2: Image of basic WPT circuit

$$L_{eq} = \frac{1}{\frac{1}{L_1} + \frac{1}{L_2} + \cdots + \frac{1}{L_n}} \tag{4.1}$$

This principle theoretically allows for inductors in parallel to be switched on and off to achieve a desired resonant frequency for the system. By having several inductors in parallel with a switching mechanism, the resonant frequency of the WPT system could be switched between a series of calculated resonant frequencies. A schematic of the theoretical frequency switching WPT system is shown in Figure 4.3.

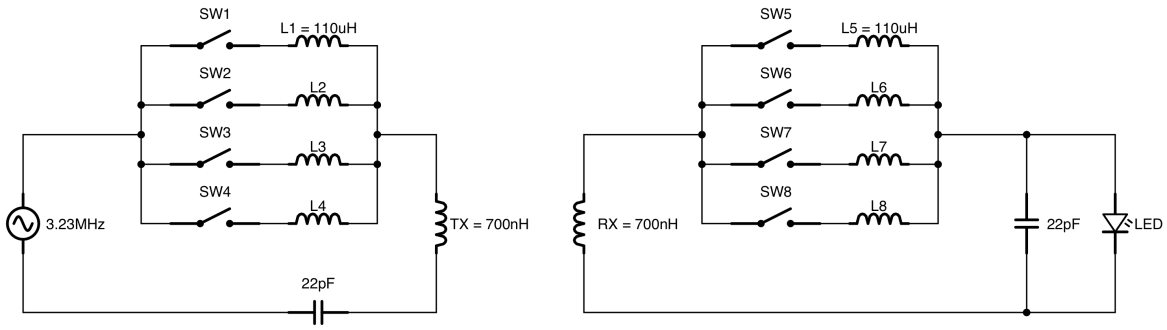

Figure 4.3: Schematic of the frequency switching WPT system

4.2.3 Manual Inductor Switching

The next logical step was to prove that switching the inductors on and off, by opening and closing the parallel rungs of the circuit, actually changed the equivalent inductance and the resonant frequency of the system. We first did this manually by connecting and disconnecting a wire between the inductive elements and the node connecting all of the elements. This procedure was successful and we verified that the resonant frequency changes when opening and closing the subcircuits that contain individual, axial inductors. We then added a bank of eight, dual in-line package (DIP) switches to the breadboard. We intended to manually switch the DIP switches and adjust the dial on the function generator to the calculated resonant frequency so as to achieve continuous WPT through a crude frequency switching mechanism. An image of this circuit can be seen in Figure 4.4.

When switching these DIP switches on and off, however, we found that the measured resonant frequency did not match the calculated resonant frequency, leading us to believe that the inductors were not completely isolated due to the breadboard or DIP switches. We then isolated each inductor on its own miniature breadboard to electrically and spatially isolate

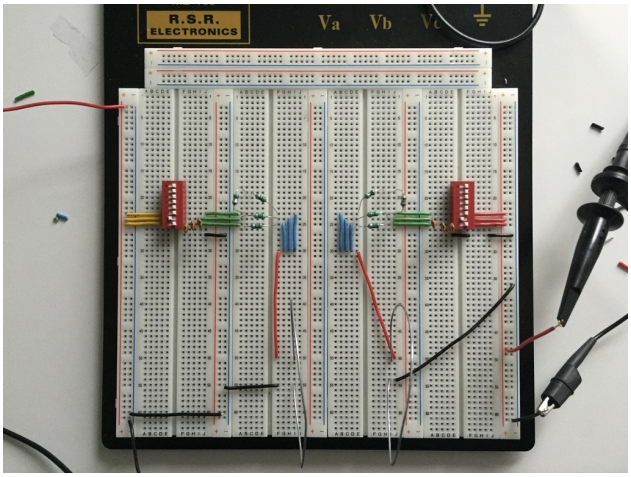

Figure 4.4: Frequency switching WPT system using DIP switches

the elements. This approach aided in removing issues inherent to breadboards, but we still found issues in using the DIP switches.

4.2.4 Digital Inductor Switching

We decided upon using NPN transistors as electrical switches to control the equivalent inductance. Again, we found there was some leakage that caused discrepancies between the measured and calculated resonant frequencies. At this point, having established that manually opening and closing the inductor subcircuit properly adjusts the resonant frequency of the system, we added mechanical relays in place of the NPN transistors. Mechanical relays allowed us to automate the process of manually opening and closing the inductor subcircuits. This means of switching had no issues and we found that the measured and calculated resonant frequencies matched. The relays we used can be seen in the center of Figure 4.5.

4.3 Transmitter Frequency Switching

Having successfully proved the frequency switching approach to WPT, we needed to remove the function generator from the transmitter side of the system in favor of a less costly device with a smaller footprint. We decided upon the incorporation of a voltage-controlled oscillator (VCO) integrated circuit to allow us to output a waveform at a specific frequency, depending on the voltage input to the chip. The VCO we selected had a range of roughly 1 MHz to 25

MHz. A schematic of the VCO is shown in Figure 4.6.

Next, we mapped the resonant frequencies of the inductors to the input voltage required to generate a waveform of the same frequency from the VCO. We found that we could effectively switch between a variety of frequencies by providing the VCO with a specific voltage and varying that voltage over time. Assuming proper synchronization of the transmitter's frequency switching with the receiver's inductor switching, wireless power transfer would not cease, even when switching to a new state. It should be noted that the VCO required selection of an external capacitor to help establish a stable frequency range and output. The capacitor we selected did not appear to generate an ideal square waveform, as made apparent by Figure 4.7.

The signal received by the receiver circuit, however, did not seem to suffer as a result of the poor waveform generated by the transmitter. The received signal is shown in Figure 4.8. In future research, consideration should be given to the VCO and external capacitor selection.

4.4 Gatekeeping Through Pseudorandom Processes

At this point in our thesis work, having proved that frequency switching allows for a WPT system to maintain multiple resonant frequencies, we changed gears to focus on the digital portion of the thesis. The goal of this thesis was to create a basic gatekeeping mechanism that functioned to digitally grant access to an analog power source; a user would be able to input a password to gain access to the WPT hub. The initial proposed means of accomplishing this was to incorporate linear feedback shift registers (LFSRs) into the system to ensure that the

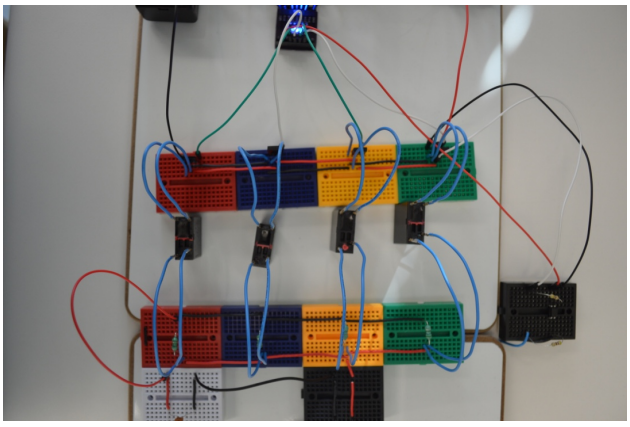

Figure 4.5: Mechanical relays used for frequency switching

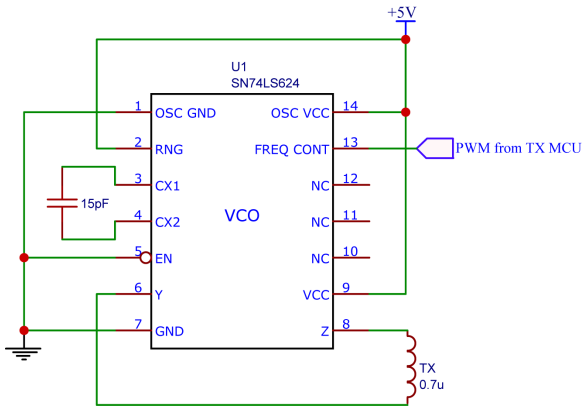

Figure 4.6: Pin diagram of the VCO in the transmitter circuit

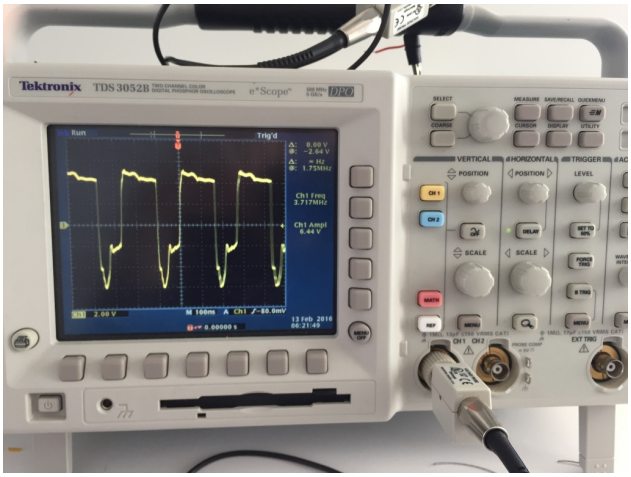

Figure 4.7: Waveform generated by the VCO

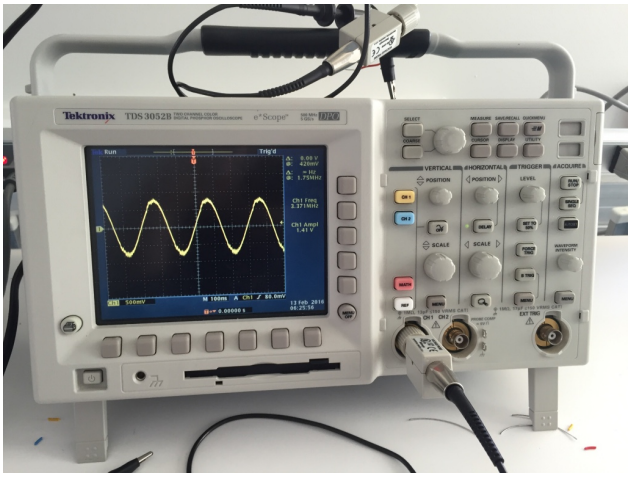

Figure 4.8: Waveform received by the receiver

transmitter and receiver both switch frequencies at a specific instance and synchronously

move through a series of predetermined frequencies. We proposed that the transmitter's LFSR be seeded with a value to generate a sequence of states, each state corresponding to a designated frequency. By seeding the receiver with the same value, an identical sequence would be generated. Once the sequence had been generated on both the transmitter and receiver, the receiver would wait in the first state until it detected power transfer from the transmitter. Because the frequencies were to be predetermined, we knew that, eventually, the transmitter would reach the first state again and both devices could begin clocking through the states together.

4.4.1 LFSR in Hardware

We first attempted to create this pseudorandom mechanism through hardware, using a shift register and XOR gates. When using hardware, we found it difficult to properly seed the shift register and began looking into alternatives. The initial hardware approach can be seen in Figure 4.9.

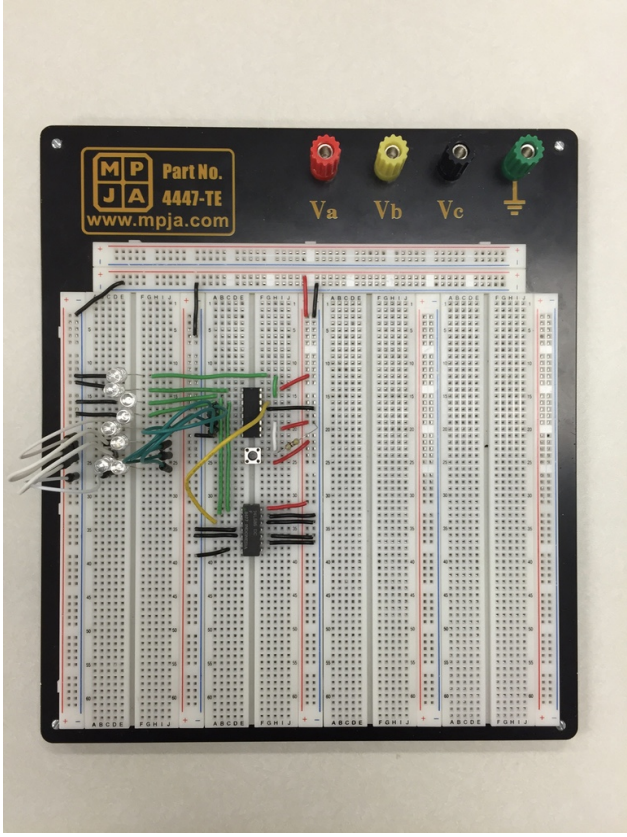

Figure 4.9: Linear feedback shift register circuit on a breadboard

4.4.2 LFSR in Software

Rather than endeavor to debug the hardware circuit, we transitioned to a software approach, writing a simple piece of C++ code to generate a sequence of states using XORs in software. This piece of code can be found in Appendix A.1. It didn't take long to realize this approach was fundamentally flawed; regardless of the seed, the sequence that was generated by the LFSR always progressed from state to state in the exact same order. The seed only controlled which state was first within that sequence. Once the sequence repeated, which was a necessary feature of the system we intended to create, the progression of states was always the same, regardless of the seed. After recognizing this behavior was inherent in LFSRs, we began looking into how we could alter the progression of states generated by the device. LFSRs function by using an XOR gate between two bits of the shift register itself. The location of the XOR gate is called a tap. There have been many studies in the past on what location to tap, depending on the length of the shift register. These studies have found which tap locations produce the maximal length sequence. Unfortunately, varying the tap location dynamically can result in a fluctuating maximal length and can even lead to the LFSR finding itself in the zero state, from which there is no return because (0 XOR N) is always 0, where N can be either 0 or 1. If the LFSR falls into an absorbing state, it will never be able to leave that state, which would prevent our system from continuing to cycle through a sequence of frequencies. At this point, we realized that LFSRs were not the solution to incorporate the pseudorandom behavior we desired in our system.

4.4.3 Rand Function in the C Library

While contemplating how to incorporate a digital frequency switching system, and having just created a software-based LFSR in C++, we decided to look into using a microcontroller unit (MCU), as it can be easily programmed in C/C++ and would be able to handle toggling outputs depending on its current state. Prior to developing firmware for the MCU, we developed a simple C program to test the functionality of the rand function provided by the C library. The code can be found in Appendix A.2. The rand function returns a pseudorandom number between 0 and, at least, 32767. By using the modulus operator, we were able to generate a number between 0 and our maximum number of states, N. The value generated was stored in an array of length N. As the array is being filled, if a number is generated that is already in the array, a new number is generated to ensure there are no duplicates within the array. By seeding the random number generator, we are able to guarantee that, no matter the computer, the code will generate an identical sequence. In

this manner, the seed can act as a password to allow for two different devices to have the same randomly generated sequence of states. The C program we wrote allows for any value to be the seed and generates a sequence of states for a four bit system. Each bit of the system corresponds to the state of an inductor; a zero bit value indicates the inductor is open and a one bit value indicates the inductor is closed. This setup results in 15 unique states, each with a corresponding resonant frequency, due to the equivalent inductance of the enabled inductors. At this point, having developed a pseudorandom, gatekeeping system and a frequency switching system, we decided to move toward integrating these two core components of our thesis to prove the concept of WPT encryption.

4.5 WPT System Hardware

To assist in the development of the WPT encryption system, we used a product called μModūls (Micro Modules). This product consists of a series of common circuit components broken out on PCBs. The modules that we used for the WPT system were as follows:

- MainModūl
- PowerModūl
- SevenSegmentModūl
- PotentiometerModūl
- SwitchModūl
- LEDModūl

The MainModūl contains an Atmel ATmega328P microcontroller which is programmed using an in-system programmer. The PowerModūl contains a voltage regulator that regulates a 9V AC/DC regulator output to 5V. The SevenSegmentModūl uses SPI to display up to four seven-segment digits. The PotentiometerModūl contains a potentiometer with a plastic knob. The SwitchModūl comprises three pushbutton switches. The LEDModūl has a bank of five surface-mount blue LEDs. Using these breakout boards, as well as some additional circuit components, we developed both a transmitter and receiver circuit that allow for secure wireless power transfer. The entire system can be seen in Figure 4.10. A block diagram of the WPT system is shown in Figure 4.11.

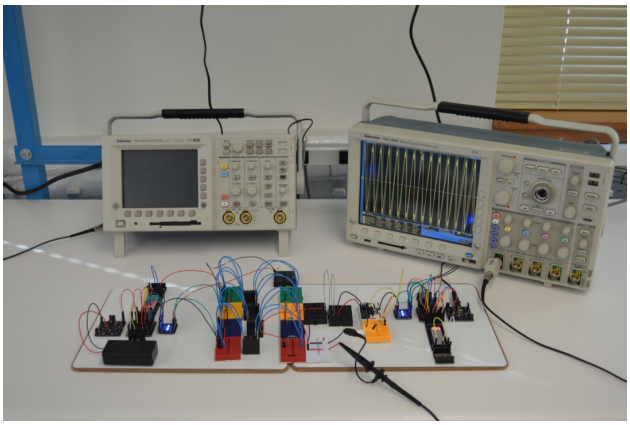

Figure 4.10: Overall WPT system

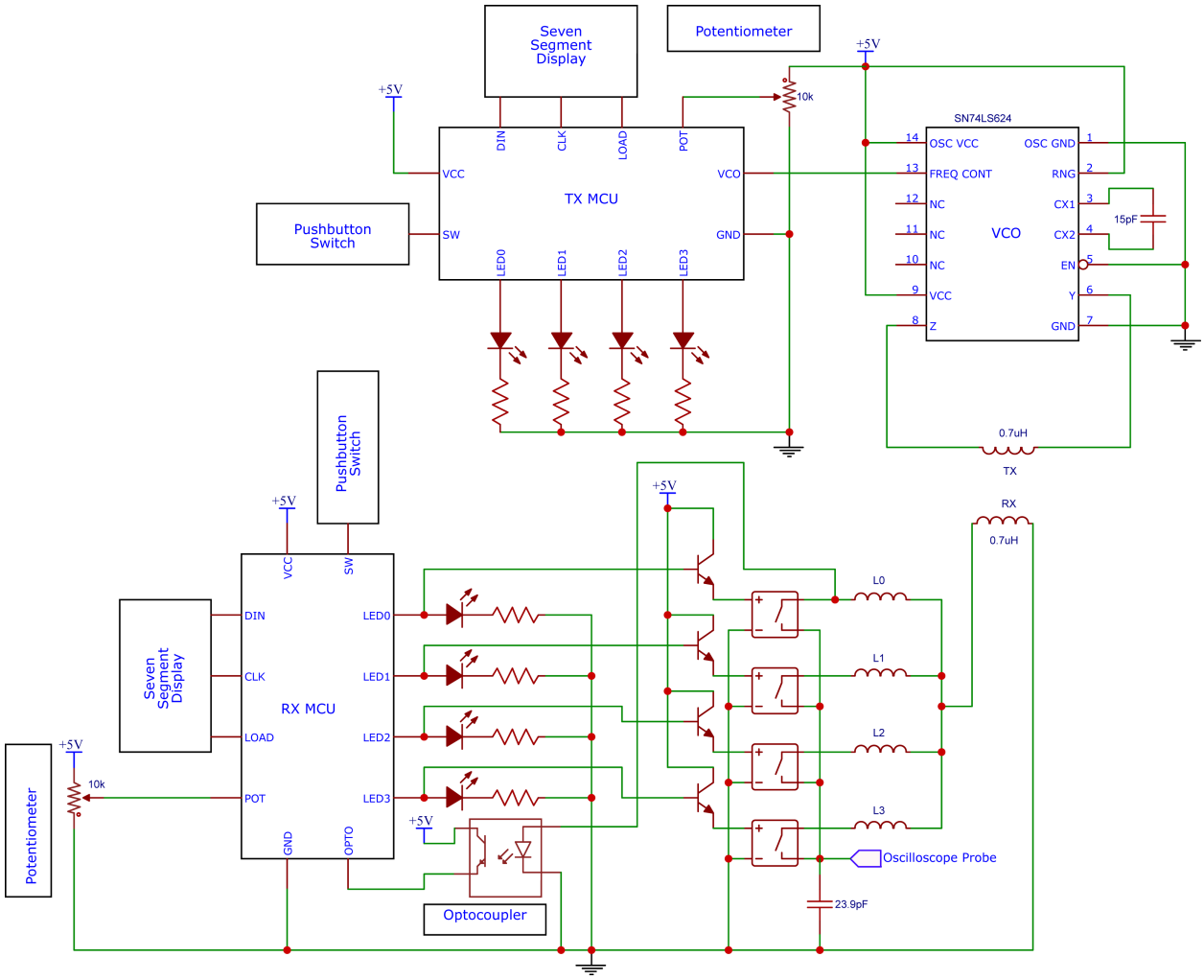

Figure 4.11: Diagram of the controlled-access WPT system

4.5.1 Transmitter Hardware

The transmitter is comprised of a MainModūl (MCU), PowerModūl, SevenSegmentModūl, PotentiometerModūl, SwitchModūl, LEDModūl, VCO, a low-pass filter, and the TX coil. An image of the transmitter circuit can be seen in Figure 4.12.

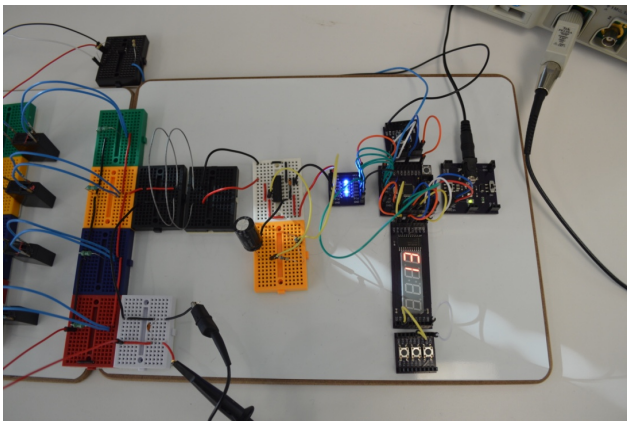

Figure 4.12: Transmitter circuit

4.5.2 Receiver Hardware

The receiver is comprised of a MainModūl (MCU), PowerModūl, 9V battery holder, SevenSegmentModūl, PotentiometerModūl, SwitchModūl, LEDModūl, four mechanical relays, an optocoupler, RX coil, and an oscilloscope. An image of the receiver circuit can be seen in Figure 4.13.

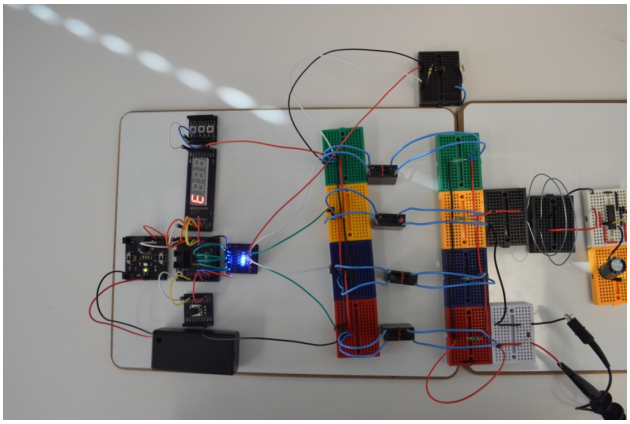

Figure 4.13: Receiver circuit

4.6 Software

After completing the hardware setup, we began writing firmware for both MCUs to handle the frequency switching and encryption processes.

4.6.1 Transmitter Operation

The transmitter was designed so that, when it turns on, the seven segment display shows a number between one and 32. This can be adjusted by turning the potentiometer. Once the user has decided on a "password" for the system, they press a pushbutton switch and that number is set as the random seed for the random number generator. The system now switches to its transmission mode, where it will begin to cycle through each of the 15 states in its randomly generated sequence. The LEDs are each connected to an output pin to illustrate the current state in binary. The seven segment display will also show the current state in Arabic numerals. As soon as the microcontroller switches states, the LED and seven segment displays update to reflect the changes. Depending on the state, the VCO outputs a different waveform directly to the TX coil. Previously, we mentioned that the VCO generates unique waveforms by varying its input voltage. Because of the digital nature of microcontrollers, we had to simulate a varying input voltage using a pulse-width modulated (PWM) output on one of the pins of the MCU. In theory, this allows the VCO to 'feel' an analog voltage between 0V and 5V, resulting in a varying output waveform. In practice however, we found that the VCO responded too quickly to the PWM signals and detected the pulses as discrete 0V and 5V signals, resulting in only two frequencies. After discovering this fact, we added a low-pass filter between the PWM output and the VCO input to smooth the waveform and make it into a more analog signal. This approach was successful and enabled the VCO to output a wide range of waveform frequencies. The transmitter code can be found in Appendix A.3.

4.6.2 Receiver Operation

The receiver functions much like the transmitter; when it is powered, the seven segment display shows a number between one and 32. This number is adjusted by the potentiometer. Once the user has entered the "password" for the system, they press a pushbutton switch and that number is set as the random seed for the random number generator. Next, the system switches into reception mode, where it will "listen" to state one until it receives a waveform.

This allows for the receiver to synchronize with the transmitter. Once it has detected a waveform, it will begin clocking through each state in its randomly generated sequence at the same rate as the transmitter cycles through its sequence of states. The current state is controlled by four pins that output a logic high or logic low signal, depending on whether each bit, within the binary representation of the state, is a zero or a one. If a bit is one, the pin goes high and the relay allows the inductor to be connected to the circuit. Every time the state changes, the relays turn turn on and off to open and close the respective inductors. If the receiver's "password" matches that of the transmitter, and both are synchronized, power transfer will continue, regardless of the state. This power transfer is illustrated on an oscilloscope that is connected to the RX coil, shown in Figure 4.14.

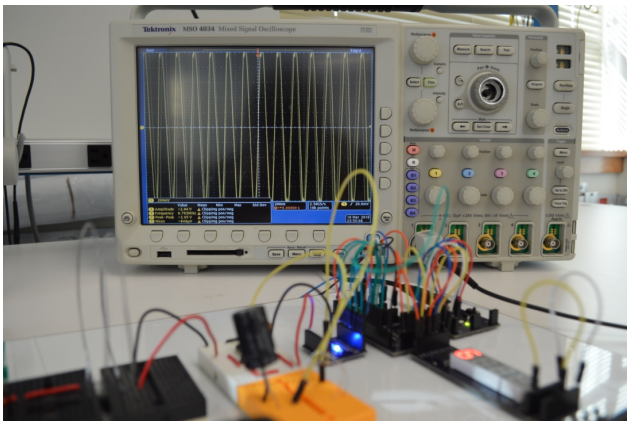

Figure 4.14: An oscilloscope displaying the received power signal

The received waveform in state one is detected by the optocoupler, which allows for complete isolation (up to 3500V) of the received waveform and the MCU. This will enable the system to function at higher power levels without damaging the receiver MCU. In our application, we wired the optocoupler to both the transmitter and receiver MCUs to simulate a waveform being detected on the RX coil. When the TX MCU enters state one, the pin connected to the emitter of the optocoupler goes high and the collector of the optocoupler detects the signal and conveys a logic high signal to the RX MCU. The optocoupler functionality had to be simulated because our proof of concept system runs at 5V and has minimal efficiency. This low power transfer and received voltage is not high enough to enable the diode within the emitter. In future applications, an amplifier circuit can be added to the transmitter to ensure enough power is received for the optocoupler to function properly, without having to be tethered to both the TX and RX MCUs. The transmitter code can be found in Appendix A.4.

4.6.3 Frequency Mapping

In order to properly map the inductors and their resonant frequencies to the VCO output via a pulse-width modulated input, the transmitter code and receiver code were modified. The receiver code was a lightly modified version of the regular receiver code. The only change was that the receiver did not wait in state one or check the optocoupler for waveform detection; it operated in continuous state-switching mode. This was accomplished by commenting out the portion of the code that checked the status of the optocoupler. The transmitter code, however, was more heavily modified. Referring to Appendix A.3, the modifications (lines 112-119) are commented out. With this code, the user could adjust the potentiometer to change the value of the pulse-width modulated signal going into the VCO. The value, between 0 and 255, was displayed on the seven segment display. By adjusting this value, as the receiver clocked through each of the 15 states, we were able to identify which PWM signal value, and ultimately VCO output frequency, mapped to which state. This was done by adjusting the potentiometer until the maximum received waveform was seen on the oscilloscope. The PWM signal value and receiver state were both recorded. We then used this map in the normal receiver code to ensure that the MCU generated PWM signals that maximized wireless power transfer to the receiver. In future development of this system, extreme care should be taken when mapping the frequencies, as the efficiency of the system is dependent on resonant frequency matching.

4.7 System Performance Evaluation

4.7.1 Experimental System Parameters

Below, several tables break out the values and parameters associated with each component within the WPT system. It should be noted that the capacitor included in the receiver has a value of 23.9 pF. The capacitor was held constant so as to reduce the number of variables contributing to the resonant frequency. From here on, this value will be referred to as the equivalent capacitance of the receiver. The equivalent capacitance is used throughout the remainder of this subsection to calculate resonant frequencies. Note that the PWM values used as inputs to the VCO are not precise; these values were determined by adjusting the potentiometer and recording the PWM value corresponding to the maximum observable power transfer, through the procedure outlined in the previous section. In future applications, special care should be taken to properly map the VCO frequency output and the resonant

frequency of the receiver.

The four inductors included in the system were chosen to allow for a broad range of resonance frequencies. This broad range was intended to prevent overlapping states. The inductance of each inductor can be seen in Table 4.1.

Inductor	**Inductance (μH)**
L_3	49.4
L_2	27.5
L_1	11.8
L_0	6.9
L_{RX}	0.7

Table 4.1: Receiver inductances

Each inductor contributes to the equivalent inductance of the receiver when it is included in the circuit by its respective relay. The status of the inductors and equivalent inductance for each state can be seen in Table 4.2.

State	L_3	L_2	L_1	L_0	$L_{eq}(\mu\text{H})$
1	0	0	0	1	7.6
2	0	0	1	0	12.5
3	0	0	1	1	5.05
4	0	1	0	0	28.2
5	0	1	0	1	6.22
6	0	1	1	0	8.96
7	0	1	1	1	4.46
8	1	0	0	0	50.1
9	1	0	0	1	6.75
10	1	0	1	0	10.22
11	1	0	1	1	4.7
12	1	1	0	0	18.37
13	1	1	0	1	5.66
14	1	1	1	0	7.77
15	1	1	1	1	4.19

Table 4.2: Equivalent inductance and enabled inductors by state

Using the equivalent inductance and equivalent capacitance, the resonant frequency for each state can be calculated. This is accomplished with the following formula:

$$f_0 = \frac{1}{2\pi\sqrt{L_{eq}C_{eq}}} \tag{4.2}$$

The resonant frequencies for each state are listed in Table 4.3.

State	$L_{eq}(\mu\text{H})$	$C_{eq}(\text{pF})$	$f_0(\text{MHz})$
1	7.6	23.9	11.81
2	12.5	23.9	9.21
3	5.05	23.9	14.48
4	28.2	23.9	6.13
5	6.22	23.9	13.06
6	8.96	23.9	10.88
7	4.46	23.9	15.42
8	50.1	23.9	4.6
9	6.75	23.9	12.53
10	10.22	23.9	10.18
11	4.7	23.9	15.01
12	18.37	23.9	7.6
13	5.66	23.9	13.68
14	7.77	23.9	11.68
15	4.19	23.9	15.9

Table 4.3: Calculated resonant frequency by state

In order for WPT via SCMR to occur, the transmitter and receiver must be in resonance. The VCO outputs a frequency, depending on its input voltage, and, using a potentiometer, the input voltage was adjusted for each state until the power transferred to the receiver was at its maximum. Maximum power transfer indicates that the transmitter and receiver are in resonance. This procedure is outlined in detail in the previous section. The corresponding VCO input and output for each state is shown in Table 4.4.

State	PWM Input (out of 255)	PWM Input (out of 5V)	Transmitter V_{pp} (V)
1	215	4.22	9.28
2	80	1.57	8.48
3	78	1.53	8.96
4	58	1.14	9.44
5	55	1.08	8.48
6	109	2.14	9.52
7	106	2.08	9.28
8	37	0.73	9.92
9	38	0.75	10.10
10	96	1.88	9.92
11	90	1.76	9.36
12	68	1.33	8.88
13	70	1.37	8.80
14	108	2.12	9.36
15	108	2.12	9.60

Table 4.4: VCO input and output voltage by state

4.7.2 Experimental System Performance

The system we designed accomplishes what we set out to prove: wireless power transfer systems can be secured, to prevent unwarranted access, while still achieving wireless power transfer. In Figure 4.15, it is clear that, when the transmitter and receiver are in the same state, meaning the receiver has "authenticated" with the transmitter, wireless power transfer is accomplished, albeit with minimal efficiency.

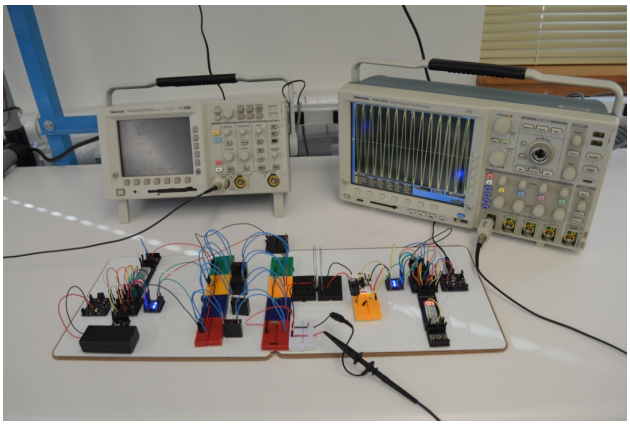

Figure 4.15: The receiver is authenticated

In Figure 4.16, the receiver and transmitter do not have the same seed, so the sequences of

states do not align, resulting in no wireless power transfer.

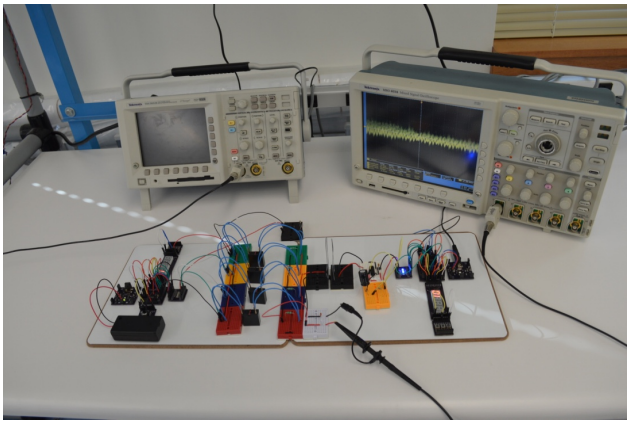

Figure 4.16: The receiver is not authenticated

The efficiency of power transfer is shown in Table 4.5. It was calculated by finding the ratio between the transmitted and received voltage.

State	**Transmitter V_{pp} (V)**	**Receiver V_{pp} (V)**	**Efficiency (%)**
1	9.28	0.64	6.90
2	8.48	2.38	28.07
3	8.96	1.78	19.87
4	9.44	1.52	16.10
5	8.48	1.46	17.22
6	9.52	1.98	20.80
7	9.28	1.18	12.72
8	9.92	1.54	15.52
9	10.10	1.64	16.24
10	9.92	1.32	13.31
11	9.36	1.68	17.95
12	8.88	0.94	10.59
13	8.80	1.96	22.27
14	9.36	2.72	29.06
15	9.60	3.14	32.71

Table 4.5: System efficiency by state

It is clear from the above table that future measures need to be taken to improve the efficiency of the secure WPT system. The minimal coil distance and low efficiency show there are many areas for improvement in the efficiency of the system.

Chapter 5

Conclusion

When we commenced working on this thesis, we began with an audit of the field. Through this initial research phase, we learned much about common means of wireless power transfer, as well as the many ways people are bringing the technology to the consumer electronics industry. As our breadth of knowledge on the subject grew, so to did our concern for the security of wireless power transfer systems. Without a mechanism to control access, anyone with an electronic device, and the proper receiver circuit, could siphon power from an unsuspecting source. This fear of power theft led us to begin developing simulations for a frequency-switching approach to wireless power transfer. After spinning our wheels with the simulation approach, we decided that experimentation would be a more conclusive approach to realizing our solution.

We began our experimentation with a basic circuit: WPT via SCMR on a breadboard. This experiment, although trivial, was crucial to our goal of building a WPT controlled-access system without assumptions. Having just moved from a simulation approach, rife with assumptions, we wanted to ensure that the system we developed was built on solid ground. In our proof of WPT via SCMR, we added our own flair to the circuit; we used an axial inductor, in series with a single-loop coil, to provide the equivalent inductance needed for resonance at a specific frequency. This was novel approach; in past research, coils have always been the primary provider for the equivalent inductance. By using axial inductors, albeit with a low quality factor, we have opened the door to incredibly planar WPT system design. Moving to planar design will allow WPT systems to be better integrated into small, often flat, consumer electronics. After proving that the inclusion of an inductive element, like an axial inductor, in series with the source coil can still enable WPT via SCMR, we decided to modify the circuit to include multiple axial inductors in parallel. The equivalent

inductance of these parallel inductors would then be in series with the source coil to provide a unique resonant frequency.

Using a wire to open and close the parallel rung of each inductor, we found that we were able to change the resonant frequency of the overall system. Manually opening and closing circuits works well in a laboratory setting, but was not conducive to our vision of an automated frequency-switching WPT system. In an effort to control the frequency-switching mechanism digitally, a sensible approach was to incorporate NPN transistors to act as electrically-controlled switches. When attempting this approach in the lab, we found that the transistors were not electrically isolated enough to provide a unique resonant frequency that matched the calculated resonant frequency for each inductor. After the setback with the transistors, we decided to move as close to manually opening and closing the inductor subcircuits as possible through the inclusion of mechanical relays. The relays were successful in switching the parallel inductors on and off, resulting in a digitally-driven frequency-switching mechanism. On the transmitter portion of the circuit, however, the function generator had to be manually dialed to the resonant frequency of the receiver in order for wireless power transfer to be achieved. We considered developing our own oscillator with an LC tank that simulated the inductor-switching behavior of the receiver, but decided to pursue the addition of a voltage-controlled oscillator (VCO) for simplicity's sake. The VCO allowed for a wide range of frequency outputs (1 MHz to 25 MHz), based on a voltage input between zero and five volts.

Having successfully proved the concept of frequency-switching on both the transmitter and receiver of the WPT system, we needed a way to control the system. The inclusion of a microcontroller in both the transmitter and receiver was essential to impart the system with the ability to switch between different frequencies automatically. The microcontroller on the transmitter controlled the VCO via PWM. The PWM signal was run through a low-pass filter prior to reaching the VCO to make the signal more analog. The VCO would then output a frequency corresponding to the voltage it felt from the low-pass filtered, pulse-width modulated signal from the MCU. On the receiver, the MCU toggled four digital output pins to enable and disable the mechanical relays, changing the resonant frequency of the receiver. After achieving digital control of the frequency-switching mechanisms on both the transmitter and receiver, we needed to establish a means of controlling access to the transmitter.

Initially, we aspired to control access to the WPT system by using linear feedback shift registers (LFSRs) to generate a sequence of states, with the binary representation of each

state corresponding to the status of the relays in the receiver. If a bit contained a one, the relay was to be enabled; a zero bit value was to disable the relay. This approach would allow the receiver to receive power in each state, provided the transmitter was transmitting at the current resonant frequency of the receiver. In essence, the two devices—transmitter and receiver—were to have matching resonant frequencies or power transfer would naturally cease. Unfortunately, due to the nature of LFSRs, the sequence of states generated could not be altered, regardless of the initial value or seed provided to the LFSR. This led us to pivot and consider using a different means of generating a random sequence. Since we intended to use microcontrollers to handle frequency switching, we decided to look into the C library's rand function. We found that, by providing the random number generator with a seed value, we could guarantee a specific sequence as the output. Providing both the transmitter and receiver MCUs with the same seed results in the exact same random sequence being generated by both devices. This functionality allows for the seed to become a "password" of sorts. If a receiver does not have the same seed as the transmitter, the sequence of states will not remotely match that of the transmitter.

With controlled-access and frequency-switching implemented, the final missing component of our system was synchronization. Even if the transmitter and receiver both had the same seed, if the two devices were not synchronized in time and state, power transfer would never occur. We determined that the best way for synchronization to occur would be to have the receiver remain in a designated state until it receives power, meaning that the transmitter has reached the matching state and the two devices are in resonance. We opted to install an optocoupler to detect power transfer in state one and then convey a signal to the receiver MCU to begin pulsing through its sequence of states. Assuming the transmitter and receiver have the same seed, power transfer will perpetually occur. Additionally, in the event that one of the devices drifts out of synchronization, the receiver will just wait in state one until it receives power again. This functionality allows for the devices to automatically "reconnect" if synchronization is lost.

Finally, we incorporated potentiometers, pushbutton switches, and seven segment displays into both the transmitter and receiver. These components allow users to adjust the seed value or "password" for the system, set the seed value, and display the seed value (until it is set) or the current state of the device (once the seed has been set). The incorporation of these inputs and outputs makes the system much more usable and conducive to integration into consumer electronics.

In summary, by completing the proof of concept outlined in this paper, we have demonstrated that wireless power transfer systems can be secured to prevent unwarranted access. Through this research, we found that axial inductors used in series with a single-loop coil can accomplish WPT via SCMR. Additionally, axial inductors used in parallel allow us to switch between multiple resonance points within a single, WPT system. Optocouplers or other power sensing devices can be incorporated into our controlled-access, WPT system to ensure synchronized frequency-switching between transmitter and receiver. Finally, both transmitter and receiver MCUs can have their random number generators seeded with identical values to generate identical sequences of states, which allows for uninterrupted wireless power transfer, assuming the devices have been properly synchronized.

Without properly securing wireless power transfer systems, power theft can easily occur and will result in unnecessary disputes. Although wireless power is not pervasive today, it has the potential to become an incredibly ubiquitous technology. Should that day come, it is imperative that there be established, preemptive security systems to prevent unauthorized access. It is our sincere hope that this research provides a base for the development of more sophisticated means of wireless power transfer security.

Chapter 6

Future Work

The intent of this thesis was to prove the concept of applying a controlled access system to wireless power transfer. Although we successfully proved the concept, there are a striking number of viable directions to take the research in the coming months and years. By focusing on three core areas, this concept can be developed into a marketable consumer electronic, ready for integration into peoples' lives. These core areas comprise:

1. Improved Efficiency
2. More Robust Security
3. Design Thinking

6.1 Improved Efficiency

The efficiency of the WPT encryption system must be improved for such a system to become commonplace. The system outlined in the previous chapters did not implement any techniques to improve the distance nor efficiency between the transmitter and receiver, resulting in a meager 1 cm coil separation, shown in Figure 6.1.

There have been many publications in the past decade that discuss how to improve the efficiency of WPT systems; an oft cited technique is impedance matching. We recommended that future researchers use impedance matching to increase the distance and efficiency of the system. These researchers should also delve into quality factor, and determine the best means of improving it, within our system, such that the system can maintain a small footprint for integration into common consumer electronics. Additionally, an amplifier circuit

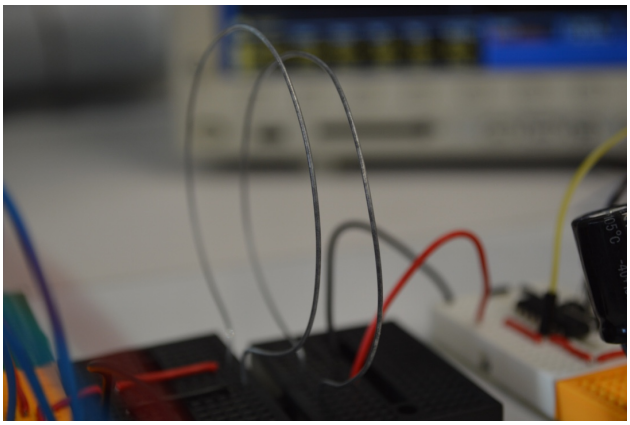

Figure 6.1: TX and RX coils

should be incorporated into the design to provide useful voltage levels, rather than the trivial power transmission that was realized in the proof of concept. Finally, an application-specific oscillator should be designed to cater to the target frequencies of the system. We recommend designing a Clapp oscillator due to its frequency stability. The oscillator should maintain the ability to switch on and off inductive elements within the LC tank to generate a specific output frequency that will mirror the frequency of a given state on the receiver. By matching the transmitter and receiver inductors, a higher quality factor and, ultimately, more efficient wireless power transfer system can be achieved.

6.2 More Robust Security

Security is an incredibly crucial component of this system. We designed our system to utilize four inductors to generate 15 unique states, each with a corresponding resonant frequency. In our proof of concept, the choice of inductors created frequencies that were very close to one another, reducing the number of truly unique states. In future development of this system, inductors must be carefully selected to allow disparate states, so as to maximize the number of truly unique states. It is also important to note that the voltage controlled oscillator (VCO) we incorporated into the transmitter did not have a linear frequency range, resulting in some error in matching the transmitter frequency with the calculated resonant frequency of the receiver. In future development, researchers should endeavor to optimize the output of the current VCO, replace the VCO with a better-suited VCO, or design a Clapp oscillator as is outlined in the previous subsection.

An easily implementable security improvement could also come in the form of an increased

number of states and unique resonant frequencies. This can be achieved by increasing the number of inductors on the receiver (and transmitter, if building a Clapp oscillator). The number of states is given by the relationship $2^n - 1$, where n is the number of inductors in the system. An increase in the number of states will decrease the relative amount of time spent in each unique state. This makes it more difficult to detect the frequencies and order of the states. A final suggested security improvement is the addition of a second "layer of encryption", in which the password that is used to seed the random number generator is used to generate an additional array of random values that, when multiplied by an array of base time durations (i.e. one second per state; $\begin{bmatrix} 1 & 1 & \dots & 1 \end{bmatrix}$) generate an array containing time durations for each state. When the system is clocking through the states, instead of a standard 1 second duration for each state, the duration will be determined by the value from the array of random time durations. By varying the duration of each state, it becomes much more difficult for an unwarranted individual to "sniff" each frequency, mirror the progression of states, and receive power from the transmitter.

6.3 Design Thinking

The final area of consideration for future development of this secure WPT system is general design thinking; in order for this proof of concept to be adapted to better suit consumer electronics applications, substantial consideration should be given to designing an easily usable, robust, yet small, WPT system that can be embedded in a wide range of products. Usability will come in the form of an easily-understandable user interface in which buttons, knobs, and switches are clearly documented, and not so prevalent as to confuse the end user. The optimal, base system will contain a screen to display relevant information, a knob or keyboard for password input, and a button to set the password. Later on, a hardware abstraction, by means of software, should be considered so that a user can connect to the WPT source through his device's operating system.

Development of a device that maintains a very small footprint, but still remains functional, is crucial to any modern consumer electronic. The small footprint can be achieved through the strategic design of a printed circuit board (PCB) that contains the components required for WPT. These components should be surface-mount devices (SMD) so as to further reduce the footprint. Additionally, future researchers should consider moving from using mechanical relays for switching states to solid state relays or electrically isolated transistors. Either of these components would provide the same switching mechanism, but with a smaller footprint

and silent operation. Research should also be completed on the feasibility of using a PCB trace as the transmitter or receiver coil. This would allow the device to be entirely planar, which significantly reduces the spaces it occupies. The final design considerations deal with the electronics within the system.

Within the receiver, a battery is used to power the receiver MCU. Given that the system enables wireless transmission of power, a subcircuit should be included that allows the power received from the transmitter to be used to recharge the battery. Researchers should also look into high-speed optocouplers, which would allow the receiver to detect wireless power transfer much faster. This would result in better synchronization and reduce the likelihood that the transmitter and receiver drift out of sync due to slight differences in their MCU clocks. Additionally, researchers should develop a more sophisticated means of synchronizing the transmitter and receiver. The optocoupler method is an incredibly analog means of synchronizing the system; future research should include an audit of available RF communication technologies to provide constant synchronization between transmitter and receiver.

It is clear from the basic proof of concept outlined in this paper that WPT security has a long way to go before it becomes as ubiquitous and robust as Wi-Fi for Internet connectivity. However, by pursuing the suggested future developments outlined above, this concept could advance very quickly and become ready for market soon thereafter. Our suggestions regarding improvements to the efficiency, security, and design of the WPT encryption system are only intended to be a starting point; considerable effort should be put forth to ensure that this system works with common consumer electronics, is intuitive to use by someone who has never utilized WPT, and, above all, is safe for the end user. Given the design considerations and suggestions outlined above, we are confident that wireless power sources can be successfully protected from unauthorized users, while still providing efficient power transfer to all of your most coveted devices.

Appendix A

Programs

A.1 Linear Feedback Shift Register Code

```
#include <iostream>

using namespace std;

// Variable declaration
int seed;
int bin_output[4];
int bin_seed[4];
int SR_1;
int SR_2;
int SR_3;
int SR_4;

// Function prototype
void printArray(int *array);

// Main function
int main(int argc, char *argv[]) {

  // Take command line input as the seed value
  if (argc > 1) {
    seed = atoi(argv[1]);
  }

  // Display the seed value
  cout << "Linear Feedback Shift Register" << endl;
```

```
27    cout << "The seed value is " << seed << endl;
28
29    // Put binary number in array
30    for (int i = 3; i >= 0; i--) {
31      if (seed%2 > 0) {
32        bin_seed[i] = 1;
33      }
34      else {
35        bin_seed[i] = 0;
36      }
37      seed = seed/2;
38    }
39
40    // Print the array containing the binary representation of the seed
41    printArray(bin_seed);
42
43    // First shift and XOR of taps 2 and 4
44    bin_output[3] = bin_seed[2];
45    bin_output[2] = bin_seed[1];
46    bin_output[1] = bin_seed[0];
47    bin_output[0] = (bin_seed[1] ^ bin_seed[3]);
48
49    // Print the array containing the current binary
50    // representation of the value in the shift register
51    printArray(bin_output);
52
53    // If the array does not yet contain the first
54    // value (meaning it hasn't yet repeated), continue to shift and XOR
55    while (memcmp(bin_seed, bin_output, sizeof(bin_seed)) != 0) {
56      int tmp0 = bin_output[1];
57      int tmp1 = bin_output[3];
58      bin_output[3] = bin_output[2];
59      bin_output[2] = bin_output[1];
60      bin_output[1] = bin_output[0];
61      bin_output[0] = (tmp0 ^ tmp1);
62
63      // Print out the resulting binary representation
64      // of the value in the shift register
65      printArray(bin_output);
66
67    }
68
69    return 0;
```

```
}

// Print the values contained within the array corresponding
// to the binary representation of a number
void printArray(int *array) {
  for (int i = 0; i < 4; i++) {
    cout << array[i];
  }
  cout << endl;
}
```

Listing A.1: Software implementation of a linear feedback shift register

A.2 Random Sequence Generator Code

```
#include <stdlib.h>
#include <stdio.h>

// Set the number of states for the system
#define NUM_STATES 16

// Function to check whether the random value generated
// is the only one in the sequence
int check_uniqueness(int *sequence, int i) {
  int count;
  for (int j = i-1; j >= 0; j--) {
    if (sequence[i] == sequence[j]) {
      count++;
    }
  }
  if(count != 0) {
    return 0;
  }
  else {
    return 1;
  }
}

// Main function
int main(int argc, char *argv[]) {

  int seed;
```

```
  int count, x;
  int sequence[NUM_STATES];

  // Take command line input as the seed value
  if (argc > 1) {
    seed = atoi(argv[1]);
  }

  // Seed the random number generator with the user-provided value
  srand(seed);

  for (int i = 0; i < NUM_STATES; i++) {
    // Generate a random number between 1 and NUM_STATES
    sequence[i] =  rand() % NUM_STATES + 1;

    // Print the value before checking its uniqueness (for debugging
     purposes)
    printf("%d\n", sequence[i]);

    // Check whether the value is unique
    int unique = check_uniqueness(sequence, i);

    // If it's not unique, continue generating values until it is
    while(!unique) {
      sequence[i] = rand() % NUM_STATES + 1;
      printf("%d\n", sequence[i]);
      unique = check_uniqueness(sequence, i);
    }
  }

  printf( "\n" );

  // Print out the entire sequence of states
  for (int i = 0; i < NUM_STATES; i++) {
    printf("%d\n", sequence[i]);
  }

  return 0;
}
```

Listing A.2: Seeded random sequence generator

A.3 Transmitter Code

```
// Pin definitions
#define POT PC3
#define POT_PIN PINC
#define POT_PORT PORTC
#define POT_DDR DDRC

#define BUTTON_PIN PINB
#define BUTTON_PORT PORTB
#define BUTTON PB0
#define BUTTON_DDR DDRB

#define LED_DDR DDRD
#define LED_PORT PORTD
#define LED_0 PD2
#define LED_1 PD3
#define LED_2 PD4
#define LED_3 PD5

// External libraries
#include <avr/io.h>
#include <avr/interrupt.h>
#include <avr/sleep.h>
#include <avr/interrupt.h>
#include <util/delay.h>
#include <stdlib.h>

// User-provided external libraries
#include "USART.h"
#include "MAX7219.h"

// Preprocessor definitions
#define NUM_STATES 15
#define NUM_BITS 4

// PWM and state mapping
int VCO_STATES[15] = { 215, 80, 78, 58, 55, 109, 106, 37, 38, 96, 90, 68,
  70, 108, 108 };

// Function prototypes
int check_uniqueness(int *sequence, int i);
void initADC(void);
```

```
42 static inline void initTimer(void);
43 void setupADCSleepmode(void);
44 uint16_t oversample16x(void);
45
46 // Interrupts
47 EMPTY_INTERRUPT(ADC_vect);
48
49 // Global variable declarations
50 uint8_t wasButtonPressed;
51 char digitsInUse = 4;
52 uint8_t seedSelected = 0;
53
54 // Main function
55 int main(void) {
56
57   // Main function scope variables
58   int seed = 0;
59   int sequence[NUM_STATES];
60   int bin_num[4];
61
62   // Set up ADC, timer, and ADC sleep mode
63   initADC();
64   initTimer();
65   setupADCSleepmode();
66
67   // TEMPORARY!     Initialize PD0 as output to simulate power transfer to
68   // receiver. This output is fed directly into the optocoupler on the
      receiver
69   DDRD |= (1 << PD0);
70
71   // Initialize LED DDRs
72   LED_DDR |= ((1 << LED_0) | (1 << LED_1) | (1 << LED_2) | (1 << LED_3));
73
74   // Initialize POT as an input
75   POT_DDR &= ~(1 << POT);
76
77   // Initialize pull-up resistor on POT_PORT
78   POT_PORT |= (1 << POT);
79
80   // Initialize BUTTON_PORT as an input
81   BUTTON_DDR &= ~(1 << BUTTON);
82
83   // Initialize pull-up resistor on BUTTON_PORT
```

```
84    BUTTON_PORT |= (1 << BUTTON);
85
86    // SCK MOSI CS/LOAD/SS
87    DDRB |= (1 << PIN_SCK) | (1 << PIN_MOSI) | (1 << PIN_SS);
88
89    // SPI Enable, Master mode
90    SPCR |= (1 << SPE) | (1 << MSTR)| (1<<SPR1);
91
92    // Decode mode to "Font Code-B"
93    MAX7219_writeData(MAX7219_MODE_DECODE, 0xFF);
94
95    // Scan limit runs from 0.
96    MAX7219_writeData(MAX7219_MODE_SCAN_LIMIT, digitsInUse - 1);
97
98    // Set brightness of display to 2
99    MAX7219_writeData(MAX7219_MODE_INTENSITY, 10);
100
101   // Turn on the display
102   MAX7219_writeData(MAX7219_MODE_POWER, ON);
103
104   // Print zero to seven segment display
105   MAX7219_displayNumber(0);
106
107   // If the seed hasn't been selected, allow the user to select a seed
108   int temp = 0;
109   while(!seedSelected) {
110
111     // Use this code to use the potentiometer adjust the PWM output from
112     // 0 to 255 and display the value on the seven segment display
113     /* int knob = oversample16x();
114     int knob_256 = knob*256/4096;
115
116     Print knob to seven segment display
117     MAX7219_displayNumber(knob_256);
118     OCR1A = knob_256; */
119
120     // Sample the potentiometer
121     int knob = oversample16x();
122
123     // Scale the potentiometer value
124     int knob_32 = knob*32/4096 + 1;
125
126     // Print scaled value to seven segment display
```

```
127     MAX7219_displayNumber(knob_32);
128
129     // If the button is pressed, seed the random number generator with
130     // the value selected
131     if (bit_is_clear(BUTTON_PIN, BUTTON)) {
132       if (!wasButtonPressed) {
133         _delay_ms(20);
134
135         // Disable the ability to further change the seed
136         wasButtonPressed = 1;
137         seedSelected = 1;
138         seed = knob_32;
139         srand(seed);
140
141         // Generate random number sequence and check for uniqueness
142         for (int i = 0; i < NUM_STATES; i++) {
143           sequence[i] =  rand() % NUM_STATES + 1;
144           int unique = check_uniqueness(sequence, i);
145           while(!unique) {
146             sequence[i] = rand() % NUM_STATES + 1;
147             unique = check_uniqueness(sequence, i);
148           }
149         }
150       }
151       else {
152         wasButtonPressed = 0;
153       }
154     }
155   }
156
157   // Loop through sequence forever
158   while (1) {
159
160     // Convert decimal number in sequence to binary
161     // and store in a separate array
162     for (int i = 0; i < NUM_STATES; i++) {
163
164       // Temporary variable
165       int number = sequence[i];
166
167       // Set PWM to proper value for given state
168       OCR1A = VCO_STATES[number-1];
169
```

```
170         // Display PWM value
171         MAX7219_displayNumber(number);
172 
173         // If number = 1 (i.e. 0b0001), set output on PD0 to high
174         // This corresponds to the transmitter being in state 1
175         // Output is tied to the optocoupler
176         if (number == 1) {
177           PORTD |= (1 << PD0);
178         }
179         else {
180           PORTD &= ~(1 << PD0);
181 
182         }
183 
184         // Put binary number in array
185         for (int j = NUM_BITS-1; j >= 0; j--) {
186           if (number%2 > 0) {
187             bin_num[j] = 1;
188           }
189           else {
190             bin_num[j] = 0;
191           }
192           number = number/2;
193         }
194 
195         // Turn on corresponding LED for each bit of the array
196         if (bin_num[0]) {
197           LED_PORT |= (1 << LED_0);
198         }
199         else {
200           LED_PORT &= ~(1 << LED_0);
201         }
202 
203         if (bin_num[1]) {
204           LED_PORT |= (1 << LED_1);
205         }
206         else {
207           LED_PORT &= ~(1 << LED_1);
208         }
209 
210         if (bin_num[2]) {
211           LED_PORT |= (1 << LED_2);
212         }
```

```
213         else {
214           LED_PORT &= ~(1 << LED_2);
215         }
216 
217         if (bin_num[3]) {
218           LED_PORT |= (1 << LED_3);
219         }
220         else {
221           LED_PORT &= ~(1 << LED_3);
222         }
223 
224         _delay_ms(5000);
225       }
226     }
227 
228     return 0;
229 }
230 
231 // Initializes the ADC
232 void initADC(void) {
233 
234     // Set mux to ADC3
235     ADMUX |= (0b00001111 & PC3);
236 
237     // Use AVCC as reference voltage
238     ADMUX |= (1 << REFS0);
239 
240     // Set ADC clock prescaler to 64
241     ADCSRA |= (1 << ADPS1) | (1 << ADPS2);
242 
243     // Enable ADC
244     ADCSRA |= (1 << ADEN); /* enable ADC */
245 }
246 
247 // Initializes the timer
248 static inline void initTimer(void) {
249 
250     // PB1 set as an output for PWM
251     DDRB |= (1 << PB1);
252 
253     // Set none-inverting mode
254     TCCR1A |= (1 << COM1A1);
255 
```

```
256   // set Fast PWM mode, 8-bit
257   TCCR1A |= (1 << WGM10);
258   TCCR1B |= (1 << WGM12);
259
260   // Set clock prescaler to 1 (no prescaling)
261   TCCR1B |= (1 << CS10);
262
263   // Current duty cycle (out of 255)
264   OCR1A = 0;
265
266 }
267
268 // Sets up the ADC sleep mode
269 void setupADCSleepmode(void) {
270   set_sleep_mode(SLEEP_MODE_ADC); /* defined in avr/sleep.h */
271   ADCSRA |= (1 << ADIE); /* enable ADC interrupt */
272   sei(); /* enable global interrupts */
273 }
274
275 // Oversample using the ADC
276 uint16_t oversample16x(void) {
277   uint16_t oversampledValue = 0;
278   uint8_t i;
279
280   for (i = 0; i < 16; i++) {
281     sleep_mode(); /* chip to sleep, takes ADC sample */
282     oversampledValue += ADC; /* add them up 16x */
283   }
284   return (oversampledValue >> 2); /* divide back down by four */
285 }
286
287 // Checks the uniqueness of the value against the sequence
288 int check_uniqueness(int *sequence, int i) {
289   int count = 0;
290   for (int j = i-1; j >= 0; j--) {
291     if (sequence[i] == sequence[j]) {
292       count++;
293     }
294   }
295   if(count != 0) {
296     return 0;
297   }
298   else {
```

```
299     return 1;
300   }
301 }
```

Listing A.3: WPT transmitter code

A.4 Receiver Code

```
1  // Pin definitions
2  #define POT PC3
3  #define POT_PIN PINC
4  #define POT_PORT PORTC
5  #define POT_DDR DDRC
6
7  #define BUTTON_PIN PINB
8  #define BUTTON_PORT PORTB
9  #define BUTTON PB0
10 #define BUTTON_DDR DDRB
11
12 #define LED_DDR DDRD
13 #define LED_PORT PORTD
14 #define LED_0 PD5
15 #define LED_1 PD4
16 #define LED_2 PD3
17 #define LED_3 PD2
18
19 #define WPT_SENSOR_DDR DDRD
20 #define WPT_SENSOR_PIN PIND
21 #define WPT_SENSOR_PORT PORTD
22 #define WPT_SENSOR PD0
23
24 // External libraries
25 #include <avr/io.h>
26 #include <avr/interrupt.h>
27 #include <avr/sleep.h>
28 #include <util/delay.h>
29 #include <stdlib.h>
30
31 // User-provided external libraries
32 #include "USART.h"
33 #include "MAX7219.h"
34
```

```
// Preprocessor definitions
#define NUM_STATES 15
#define NUM_BITS 4

// Prototype functions
int check_uniqueness(int *sequence, int i);
void initADC(void);
void setupADCSleepmode(void);
uint16_t oversample16x(void);

// Interrupts
EMPTY_INTERRUPT(ADC_vect);

// Global variables
uint8_t wasButtonPressed;
uint8_t voltageReceived;
uint8_t incrementState;
uint8_t firstState;
char digitsInUse = 4;
uint8_t seedSelected = 0;

// Main function
int main(void) {

  // Main function scope variables
  int seed = 0;
  int sequence[NUM_STATES];
  int bin_num[4];

  // Set up ADC
  initADC();
  setupADCSleepmode();

  // Initialize LED DDRs
  LED_DDR |= ((1 << LED_0) | (1 << LED_1) | (1 << LED_2) | (1 << LED_3));

  // Initialize POT as an input
  POT_DDR &= ~(1 << POT);

  // Initialize pull-up resistor on POT_PORT
  POT_PORT |= (1 << POT);

  // Initialize BUTTON_PORT as an input
```

```
78    BUTTON_DDR &= ~(1 << BUTTON);
79
80    // Initialize pull-up resistor on BUTTON_PORT
81    BUTTON_PORT |= (1 << BUTTON);
82
83    // Initialize WPT_SENSOR_PORT as an input
84    WPT_SENSOR_DDR &= ~(1 << WPT_SENSOR);
85
86    // Initialize pull-up resistor on WPT_SENSOR_PORT
87    WPT_SENSOR_PORT |= (1 << WPT_SENSOR);
88
89    // SCK MOSI CS/LOAD/SS
90    DDRB |= (1 << PIN_SCK) | (1 << PIN_MOSI) | (1 << PIN_SS);
91
92    // SPI Enable, Master mode
93    SPCR |= (1 << SPE) | (1 << MSTR)| (1<<SPR1);
94
95    // Decode mode to "Font Code-B"
96    MAX7219_writeData(MAX7219_MODE_DECODE, 0xFF);
97
98    // Scan limit runs from 0.
99    MAX7219_writeData(MAX7219_MODE_SCAN_LIMIT, digitsInUse - 1);
100
101   // Set brightness of display to 2
102   MAX7219_writeData(MAX7219_MODE_INTENSITY, 10);
103
104   // Turn on the display
105   MAX7219_writeData(MAX7219_MODE_POWER, ON);
106
107   // Print zero to seven segment display
108   MAX7219_displayNumber(0);
109
110   // If the seed hasn't been selected, allow the user to select a seed
111   while(!seedSelected) {
112
113     // Sample the potentiometer
114     int knob = oversample16x();
115
116     // Scale the potentiometer value
117     int knob_32 = knob*32/4096 + 1;
118
119     // Print scaled value to seven segment display
120     MAX7219_displayNumber(knob_32);
```

```
121
122     // If the button is pressed, seed the random number generator with
123     // the value selected
124     if (bit_is_clear(BUTTON_PIN, BUTTON)) {
125       if (!wasButtonPressed) {
126         _delay_ms(20);
127
128         // Disable the ability to further change the seed
129         wasButtonPressed = 1;
130         seedSelected = 1;
131         seed = knob_32;
132         srand(seed);
133
134         // Generate random number sequence
135         for (int i = 0; i < NUM_STATES; i++) {
136           sequence[i] =  rand() % NUM_STATES + 1;
137           int unique = check_uniqueness(sequence, i);
138           while(!unique) {
139             sequence[i] = rand() % NUM_STATES + 1;
140             unique = check_uniqueness(sequence, i);
141           }
142         }
143       }
144       else {
145         wasButtonPressed = 0;
146       }
147     }
148   }
149
150   // Loop through sequence forever
151   while (1) {
152
153     // If we are incrementing states, make sure that we start
154     // at the beginning of the sequence of states
155     if (incrementState) {
156       firstState = 0;
157     }
158     // Otherwise, start at the location of state 1
159     else {
160       for (int i = 0; i < NUM_STATES; i++) {
161         if (sequence[i] == 1) {
162           firstState = i;
163           break;
```

```
164         }
165       }
166     }
167
168     // Only begin incrementing states if it is known that the transmitter
169     // just entered the state 1 (from the optocoupler)
170     while(!incrementState) {
171       if (bit_is_clear(WPT_SENSOR_PIN, WPT_SENSOR)) {
172         if (!voltageReceived) {
173           voltageReceived = 1;
174           incrementState = 1;
175         }
176       }
177       else {
178         voltageReceived = 0;
179       }
180     }
181
182     // Convert decimal number in sequence to binary
183     // and store in a separate array
184     for (int i = firstState; i < NUM_STATES; i++) {
185
186       // Temporary variable
187       int number = sequence[i];
188
189       // Display current state
190       MAX7219_displayNumber(number);
191
192       // Correction to re-sync when clocks are out of sync
193       if (number == 1) {
194         if (bit_is_set(WPT_SENSOR_PIN, WPT_SENSOR)) {
195           voltageReceived = 0;
196           incrementState = 0;
197           LED_PORT &= ~((1 << LED_0) | (1 << LED_1) \
198           | (1 << LED_2) | (1 << LED_3));
199         }
200       }
201
202       // If we are currently incrementing states, convert
203       // the number to binary and store in an array
204       if (incrementState) {
205         // Put binary number in array
206         for (int j = NUM_BITS-1; j >= 0; j--) {
```

```
207           if (number%2 > 0) {
208             bin_num[j] = 1;
209           }
210           else {
211             bin_num[j] = 0;
212           }
213           number = number/2;
214         }
215
216         // Turn on corresponding LED for each bit of the array. The LEDs
    are
217         // each connected to a relay, so the inductors can be enabled and
218         // disabled.
219         if (bin_num[0]) {
220           LED_PORT |= (1 << LED_0);
221         }
222         else {
223           LED_PORT &= ~(1 << LED_0);
224         }
225
226         if (bin_num[1]) {
227           LED_PORT |= (1 << LED_1);
228         }
229         else {
230           LED_PORT &= ~(1 << LED_1);
231         }
232
233         if (bin_num[2]) {
234           LED_PORT |= (1 << LED_2);
235         }
236         else {
237           LED_PORT &= ~(1 << LED_2);
238         }
239
240         if (bin_num[3]) {
241           LED_PORT |= (1 << LED_3);
242         }
243         else {
244           LED_PORT &= ~(1 << LED_3);
245         }
246
247         // Duration of each state
248         _delay_ms(5000);
```

```
      }
    }
  }
  return 0;
}

// Initializes the ADC
void initADC(void) {

  // Set mux to ADC3
  ADMUX |= (0b00001111 & PC3);

  // Use AVCC as reference voltage
  ADMUX |= (1 << REFS0);

  // Set ADC clock prescaler to 64
  ADCSRA |= (1 << ADPS1) | (1 << ADPS2);

  // Enable ADC
  ADCSRA |= (1 << ADEN); /* enable ADC */
}

// Sets up the ADC sleep mode
void setupADCSleepmode(void) {
  set_sleep_mode(SLEEP_MODE_ADC); /* defined in avr/sleep.h */
  ADCSRA |= (1 << ADIE); /* enable ADC interrupt */
  sei(); /* enable global interrupts */
}

// Oversample using the ADC
uint16_t oversample16x(void) {
  uint16_t oversampledValue = 0;
  uint8_t i;

  for (i = 0; i < 16; i++) {
    sleep_mode(); /* chip to sleep, takes ADC sample */
    oversampledValue += ADC; /* add them up 16x */
  }
  return (oversampledValue >> 2); /* divide back down by four */
}

// Checks the uniqueness of the value against the sequence
int check_uniqueness(int *sequence, int i) {
```

```
292   int count = 0;
293   for (int j = i-1; j >= 0; j--) {
294     if (sequence[i] == sequence[j]) {
295       count++;
296     }
297   }
298   if(count != 0) {
299     return 0;
300   }
301   else {
302     return 1;
303   }
304 }
```

Listing A.4: WPT receiver code

A.5 User-provided External Libraries

MAX7219 Driver Header File

```
1  // Outputs, pin definitions
2  #define PIN_SCK                    PB5
3  #define PIN_MOSI                   PB3
4  #define PIN_SS                     PB2
5
6  #define ON                         1
7  #define OFF                        0
8  #define MAX_DIGITS                 4
9
10 #define MAX7219_LOAD1              PORTB |= (1<<PIN_SS)
11 #define MAX7219_LOAD0              PORTB &= ~(1<<PIN_SS)
12
13 #define MAX7219_MODE_DECODE        0x09
14 #define MAX7219_MODE_INTENSITY     0x0A
15 #define MAX7219_MODE_SCAN_LIMIT    0x0B
16 #define MAX7219_MODE_POWER         0x0C
17 #define MAX7219_MODE_TEST          0x0F
18 #define MAX7219_MODE_NOOP          0x00
19
20 // I only have 3 digits, no point having the
21 // rest. You could use more though.
```

```
#define MAX7219_DIGIT0            0x01
#define MAX7219_DIGIT1            0x02
#define MAX7219_DIGIT2            0x03
#define MAX7219_DIGIT3            0x04

#define MAX7219_CHAR_BLANK        0xF
#define MAX7219_CHAR_NEGATIVE     0xA

void spiSendByte (char databyte);

void MAX7219_writeData(char data_register, char data);

void MAX7219_clearDisplay(void);

void MAX7219_displayNumber(volatile long number);
```

Listing A.5: MAX7219 Driver Header File

MAX7219 Driver C File

```
#include <avr/io.h>
#include "MAX7219.h"

void spiSendByte (char databyte) {
    // Copy data into the SPI data register
    SPDR = databyte;
    // Wait until transfer is complete
    while (!(SPSR & (1 << SPIF)));
}

void MAX7219_writeData(char data_register, char data) {
    MAX7219_LOAD0;
        // Send the register where the data will be stored
        spiSendByte(data_register);
        // Send the data to be stored
        spiSendByte(data);
    MAX7219_LOAD1;
}

void MAX7219_clearDisplay(void) {
    char i = MAX_DIGITS;
    // Loop until 0, but don't run for zero
    do {
```

```
        // Set each display in use to blank
        MAX7219_writeData(i, MAX7219_CHAR_BLANK);
    } while (--i);
}

void MAX7219_displayNumber(volatile long number) {
    char negative = 0;

    // Convert negative to positive.
    // Keep a record that it was negative so we can
    // sign it again on the display.
    if (number < 0) {
        negative = 1;
        number *= -1;
    }

    MAX7219_clearDisplay();

    // If number = 0, only show one zero then exit
    if (number == 0) {
        MAX7219_writeData(MAX7219_DIGIT0, 0);
        return;
    }

    // Initialization to 0 required in this case,
    // does not work without it. Not sure why.
    char i = 0;

    // Loop until number is 0.
    do {
        MAX7219_writeData(++i, number % 10);
        // Actually divide by 10 now.
        number /= 10;
    } while (number);

    // Bear in mind that if you only have three digits, and
    // try to display something like "-256" all that will display
    // will be "256" because it needs an extra fourth digit to
    // display the sign.
    if (negative) {
        MAX7219_writeData(i, MAX7219_CHAR_NEGATIVE);
    }
}
```

Listing A.6: MAX7219 Driver C File

Bibliography

[1] T. K. Sarkar, R. J. Mailloux, A. A. Oliner, M. Salazar-Palma, and D. L. Sengupta, *History of Wireless*. Hoboken, New Jersey: Wiley-Interscience, 2006.

[2] J. C. Maxwell, *The Scientific Papers of James Clerk Maxwell*, W. D. Niven, Ed. Cambridge, UK: Cambridge University Press, 1980, vol. 1.

[3] A. Karalis, J. D. Joannopoulos, and M. Soljačić, "Efficient wireless non-radiative mid-range energy transfer," *Annals of Physics*, vol. 323, pp. 34–48, 2008.

[4] B. L. Cannon, J. F. Hoburg, D. D. Stancil, and S. C. Goldstein, "Magnetic resonant coupling as a potential means for wireless power transfer to multiple small receivers," *IEEE Transactions on Power Electronics*, vol. 24, pp. 1819–1825, 7 Jul. 2009.

[5] A. Kurs, A. Karalis, R. Moffatt, J. D. Joannopoulos, P. Fisher, and M. Soljačić, "Wireless power transfer via strongly coupled magnetic resonances," *Science*, vol. 317, pp. 83–86, 5834 Jul. 2007.

[6] D. Silva. (Dec. 2013). " 'Theft of power' lands electric-car driver in jail", NBC News, [Online]. Available: `http://www.nbcnews.com/news/other/theft-power-lands-electric-car-driver-jail-f2D11694914` (visited on 11/02/2015).

[7] E. R. Hamam, A. Karalis, J. Joannopoulos, and M. Soljačić, "Efficient weakly-radiative wireless energy transfer: An eit-like approach," *Annals of Physics*, vol. 324, pp. 1783–1795, May 2009.

[8] T. Beh, M. Kato, T. Imura, and Y. Hori, "Wireless power transfer system via magnetic resonant coupling at fixed resonance frequency – power transfer system based on impedance matching," *World Electric Vehicle Journal*, vol. 4, pp. 744–752, Nov. 2010.

[9] T. Imura and Y. Hori, "Maximizing air gap and efficiency of magnetic resonant coupling for wireless power transfer using equivalent circuit and neumann formula," *IEEE Transactions on Industrial Electronics*, vol. 58, pp. 4746–4752, 10 Feb. 2011.

[10] J. Pannier, D. Hendrickx, F. Petré, and T. Nobels, "Wireless power transfer for industrial applications through strongly coupled magnetic resonances," Master's thesis, Leuven Engineering College, Leuven, Belgium, 2011.

[11] A. Salman, A. Abbas, J. Maqbool, and K. M. L. Bhatti, "Efficient wireless electric power transmission using magnetic resonance coupling," *International Journal of Scientific & Engineering Research*, vol. 5, pp. 2235–2238, 1 Jan. 2014.

[12] T. P. Duong and J.-W. Lee, "Experimental results of high-efficiency resonant coupling wireless power transfer using a variable coupling method," *IEEE Microwave and Wireless Components Letters*, vol. 21, pp. 442–444, 8 Aug. 2011.

[13] K. A. Grajski, R. Tseng, and C. Wheatley, "Loosely-coupled wireless power transfer: Physics, circuits, standards," *Microwave Workshop Series on Innovative Wireless Power Transmission: Technologies, Systems, and Applications (IMWS), 2012 IEEE MTT-S International*, pp. 9–14, May 2012.

[14] J. Kim, W.-S. Choi, and J. Jeong, "Loop switching technique for wireless power transfer using magnetic resonance coupling," *Progress in Electromagnetics Research*, vol. 138, pp. 197–209, 2013.

[15] H. Vázquez-Leal, A. Gallardo-Del-Angel, R. Castañeda-Sheissa, F. J. González-Martínez, A. Bodrov, S.-K. Sul, Y. Park, J. Kim, K.-H. Kim, M. Dionigi, A. Costanzo, M. Mongiardo, H. Sugiyama, H. Hirayama, T. Komaru, M. Koizumi, K. Komurasaki, T. Shibata, K. Kano, I.-J. Yoon, H. Ling, R. J. Sedwick, S. Kahng, H. Hoang, F. Bien, H. H. Wu, G. A. Covic, J. T. Boys, H. L. Li, and P. A. Hu, *Wireless Power Transfer - Principles and Engineering Explorations*, K. Y. Kim, Ed. 2012, ISBN: 978-953-307-874-8.

[16] M. Truitt, "Theoretical and experimental study of frequency-selective wireless electromagnetic power transfer," Miami University, Oxford, Ohio, Senior design project report, 2007.

[17] S. M. Wentworth, *Applied Electromagnetics*. John Wiley & Sons, Inc., 2007, ISBN: 978-0-470-04257-1.

[18] M. N. O. Sadiku and C. K. Alexander, *Fundamentals of Electric Circuits, Fifth Edition*. Science Engineering & Math, 2012, ISBN: 978-0073380575.

[19] R. F. Graf, *The Modern Oscillator Circuit Encyclopedia*. TAB Books, 1992, ISBN: 0-8306-3925-X.

[20] G. Gonzalez, *Foundations of Oscillator Circuit Design*. ARTECH HOUSE, INC, 2007, ISBN: 978-1-59693-162-6.

[21] E. R. Giler, K. L. Hall, M. P. Kesler, M. Soljacic, A. Karalis, A. B. Kurs, Q. Li, and S. J. Ganem, "Wireless energy transfer using repeater resonators," US8587155B2, 2010.

[22] M. Koizumi, K. Komurasaki, Y. Mizuno, and Y. Arakawa, "Wireless power feeding with strongly coupled magnetic resonance for a flying object," *Wireless Engineering and Technology*, vol. 3, pp. 86–89, 2012.

[23] G. Lee, B. H. Waters, C. Shi, W. S. Park, and J. R. Smith, "Design considerations for asymmetric magnetically coupled resonators used in wireless power transfer applications," *IEEE Topical Conference on Biomedical Wireless Technologies, Networks, and Sensing Systems (BioWireleSS)*, pp. 151–153, 2013.

[24] Y. Kim and S. Lim, "High efficient misaligned wireless power transfer using magnetic resonant coupling and additional capacitor," *Asia-Pacific Microwave Conference Proceedings*, pp. 1049–1051, 2012.

[25] J. Wu, B. Wang, W. S. Yerazunis, and K. H. Teo, "Wireless power transfer with artificial magnetic conductors," *IEEE Wireless Power Transfer*, pp. 155–158, 2013.

[26] S. K. Rahman, O. Ahmed, M. S. Islam, A. H. M. R. Awal, and M. S. Islam, "Design and construction of wireless power transfer system using magnetic resonant coupling," *American Journal of Electromagnetics and Applications*, vol. 2, pp. 11–15, 2014.

[27] X. Wei, Z. Wang, and H. Dai, "A critical review of wireless power transfer via strongly coupled magnetic resonances," *Energies*, vol. 7, pp. 4316–4341, 2014.

[28] K. Yamaguchi, I. Hodaka, and Y. Yamamoto, "Estimation of coupling coefficient for wireless power transfer," *Recent Advances in Circuits, Communications and Signal Processing*, 2013.

[29] H. Chan, K. Cheng, and D. Sutanto, "A simplified neumann's formula for calculation of inductance of spiral coil," *Eighth International Conference on Power Electronics and Variable Speed Drives*, pp. 69–73, 2000.

[30] Z. N. Low, R. A. Chinga, R. Tseng, and J. Lin, "Design and test of a high-power high-efficiency loosely coupled planar wireless power transfer system," *IEEE Transactions on Industrial Electronics*, vol. 56, pp. 1801–1812, 2009.

[31] B. Wang, T. Nishino, and K. H. Teo, "Wireless power transmission efficiency enhancement with metamaterials," *IEEE International Conference on Wireless Informatio Technology and Systems*, pp. 1–4, 2010.

[32] B. Wang, K. H. Teo, T. Nishino, W. Yerazunis, J. Barnwell, and J. Zhang, "Wireless power transfer with metamaterials," *Proceedings of the 5th European Conference on Antennas and Propagation*, pp. 3905–3908, 2011.

[33] B. Wang, W. Yerazunis, and K. H. Teo, "Wireless power transfer: Metamaterials and array of coupled resonators," *Proceedings of the IEEE*, pp. 1359–1368, 2013.

[34] A. Sample, D. Meyer, and J. Smith, "Analysis, experimental results, and range adaptation of magnetically coupled resonators for wireless power transfer," *IEEE Transactions on Industrial Electronics*, vol. 58, pp. 544–554, 2011.

[35] T. Deyle and M. Reynolds, "Surface based wireless power transmission and bidirectional communication for autonomous robot swarms," *IEEE International Conference on Robotics and Automation*, pp. 1036–1041, 2008.

[36] G. Wang, W. Liu, M. Sivaprakasam, M. Humayun, and J. Weiland, "Power supply topologies for biphasic stimulation in inductively powered implants," *IEEE International Symposium on Circuits and Systems*, vol. 3, pp. 2743–2746, 2005.

[37] B. Jiang, J. R. Smith, M. Philipose, S. Roy, K. Sundara-Rajan, and A. V. Mamishev, "Energy scavenging for inductively coupled passive rfid systems," *IEEE Transactions on Instrumentation and Measurement*, vol. 56, pp. 118–125, 2007.

[38] C.-J. Chen, T.-H. Chu, C.-L. Lin, and Z.-C. Jou, "A study of loosely coupled coils for wireless power transfer," *IEEE Transactions on Circuits and Systems II*, vol. 57, pp. 536–540, 2010.

[39] E. Waffenschmidt and T. Staring, "Limitation of inductive power transfer for consumer application," *European Conference on Power Electronics and Applications*, pp. 1–10, 2009.

[40] X. Liu, F. Zhang, S. Hackworth, R. J. Sclabassi, and M. Sun, "Wireless power transfer system design for implanted and worn devices," *IEEE 35th Annual Northeast Bioengineering Conference*, pp. 1–2, 2009.